NTNU – Trondheim
Norwegian University of
Science and Technology

Forward Seismic Forward Modeling of an Outcrop Model from Kvalvågen on Spitsbergen

Investigating Thin Layers and Complex
Geological Structures

Knut-Gunnar Steinsbø

Petroleum Geoscience and Engineering
Submission date: July 2013
Supervisor: Ståle Emil Johansen, IPT

Norwegian University of Science and Technology
Department of Petroleum Engineering and Applied Geophysics

Abstract

In this Master's thesis a seismic modelling study has been performed on a geological outcrop at Kvalvågen on Spitsbergen. Geological and petrophysical models were made in order to simulate a seismic survey over the outcrop using forward seismic modelling. The synthetic data is then processed to seismic images aiming to study thin layers and the complex geological structures found in the outcrop.

The Petrel software was used to make the geological models and the Madagascar software package is used to acquire and process the synthetic seismic data. The geological and petrophysical models are based on an image of the outcrop and measurements from rock samples taken at the outcrop.

The final images display the improvements of reverse time migration compared to the Kirchhoff Pre-stack time migration especially in the more complex geological settings of the model. It is found that the vertical resolution is at least 5 meters in the depth migrated section and it is shown how the vertical resolution decreases with decreasing frequency content. The effects of frequency filtering on a seismic image is presented and it is shown how this might be helpful with regards to seismic interpretation.

Acquisition related dispersion effects cause some odd vertical lines in the final sections but is attributed to high frequency content and/or grid size. The final images of this thesis are of high seismic quality and this is attributed to the high frequencies in the source signal, absence of multiples, the use of perfect velocities in the processing and the homogeneous geological and

petrophysical models.

Samandrag

I denne hovudoppgåva er ei seismisk modellering utført på geologisk blottning ved Kvalvågen på Spitsbergen. Geologiske og petropfysiske modeller av blotninga vart laga og deretter nytta i ein simulert seismisk innsamling ved hjelp seimisk framover modellering. Den syntetiske dataen vart deretter prosessert til seimiske bilete med mål om å studera tynne lag og dei komplekse geologiske strukturene i blottninga.

Programvaren Petrel er nytta til å laga den geologiske og dei petropysiske modellane og Madagascar programvarepakken er nytta til å samla inn og prosessere den syntetiske seismisk dataen. Modellane i denne hovudoppgåva er laga på grunnlag av eit bilete av blottninga og målingar tatt på bergartsprøvar.

Dei endelege seismiske bileta synar fordelane med å nytta revers tid migrasjon framfor Kirchhoffs Pre-stack tidsmigrasjon særleg i dei meir komplekse delane av modellen. Den vertikale oppløysinga er funnen til å vera minimum 5 meter i den dybde migrerte seksjonen and det synast korleis den vertikale oppløysinga synk med synkande frekvens innhald. Effekten av å filtere ut visse frekvensar i eit seismisk bilete er vist og fordelane som detta kan føra til i seismisk tolkning er og vist.

Dispersjonseffektar i høve med innsamling gjev nokre merkelege vertikale linjer i dei seismiske bileta. Årsaka vert funnen til å vera ein blanding av høgt frekvens innhald og får liten gitterstorleik. Dei endelege bileta i denne hovudoppgåva er av høg seimisk kvalitet og dette vert forklart som å vera eit

resultat av høge frekvensar i kjeldesignalet, fråvær av multiplar, bruk av perfekte snøggleikar i migrasjonane og dei homogene geologiske og petrofysiske modellane.

Preface

This Mater thesis is submitted to The Department of Petroleum Engineering and Applied Geophysics at the Norwegian University of Science and Technology (NTNU).

The work has been performed from Febraury to July 2013 and was carried out at The Department of Petroleum Engineering and Applied Geophysics at the Norwegian University of Science and Technology (NTNU). Ståle Emil Johansen has been the advisor to this Master thesis.

Acknowledgments

I want to thank my advisor at The Department of Petroleum Engineering and Applied Geophysics, Ståle Emil Johansen, for guidance, advise and encouragement while working on the thesis.

Professor Børge Arntsen and PhD student Espen B. Raknes have written most of the software used for seismic modelling and processing in this thesis and I am most thankful for the work that they have done. Both of them have otherwise been most helpful whenever I have had questions or requests regarding my thesis.

I want to thank all of my fellow students and especially those at Geolabben for offering valuable advise, interesting discussions and vital encouragement during the spring.

Contents

List of Figures

List of Tables

Chapter 1

Introduction

Forward seismic modelling is a technique used in the geosciences to generate synthetic seismograms by numerically computing the displacement measured by a set of seismic receivers caused by seismic waves propagating through a geological model (Carcione, 2002; Ikelle and Amundsen, 2005; Krebes, 2004). Generating synthetic seismic sections is a tool that geoscientists can use to better interpret seismic data especially in geologically complex areas, better understand seismic wave propagation and test seismic processing and inversion algorithms (Johansen, Kibsgaard, et al., 1994; Tøndel, 1997).

The goal of this thesis is to make a geological and petrophysical models based on a image of a geological outcrop at Kvalvågen on Spitsbergen, Norway. From here seismic data will be generated by simulating seismic wave propagation and seismic images produced by processing the seismic data. The outcrop is small and on the scale of a oil and gas reservoir so this thesis aims to investigate how well thin layers can be resolved in the final image and if the all of the faults in the section will be imaged.

chapter 2 aims to give the reader a better understanding of theory behind the methods used in this thesis with an emphasis on seismic modelling. The numerical theory, emphasizing on finite difference modelling, the use forward seismic modelling in geoscience and short introduction to seismic imaging is presented.

chapter 3 will present the geological setting of the outcrop at Kvalvågen and discuss the stratigraphy and structural setting of the area.

chapter 4 should get the reader acquainted with the available data which is used in this thesis.

chapter 6 is where the results from the geological interpretation, model building, seismic modelling and seismic processing will be presented.

chapter 7 will contain the discussions on the results from chapter 6 and also include some thoughts on sources of error and potential further work.

chapter 8 is where the main findings of the thesis are summed up and conclusions are drawn.

Chapter 2

Theory

This chapter will give an introduction to the theory behind the work done in the later chapters of the thesis. A throughout introduction to Forward seismic modelling is given together with a description of the theoretical framework that the seismic modelling software used in this thesis is based on. The use of seismic modelling in geoscience is discussed and a work flow for performing seismic modelling is presented. Several of the sections presented in this chapters are modified from Steinsbø (2012).

2.1 Forward Seismic Modelling

The goal of a geophysical forward problem is to do some kind of physical experiment on a model of the earth which will produce a set of data values that corresponds to the measurements one would get from performing the same experiment in nature. An inverse problem involves recreating an earth model from measurements taken in nature, Figure 2.1 shows a simple sketch illustrating the forward and inverse problem. Forward seismic modelling uses numerical solutions of the wave equations and is used in geoscience to produce synthetic seismograms of the subsurface (Krebes, 2004). Geological models and models of physical properties of the earth, such as velocity and density of the subsurface are used to the predict travel times and amplitude data measured at a set of seismic receivers.

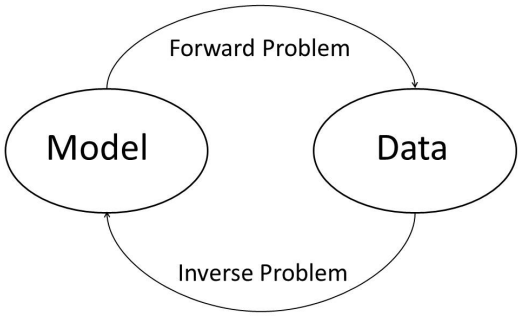

Figure 2.1: Sketch showing the inverese and forward problems

Understanding how seismic waves propagate through the earth is essential to generate good numerical solutions of wave propagation in the subsurface. Seismic wave propagation in the subsurface can be viewed as material particles in earth set in motion due to pressure waves. Newtons second law of

motion is sufficient to describe material particles of a solid body set in motion by elastic waves. The equation of motion is a second order differential equation and can also be seen as the mathematical expression of the displacement a point or particle undergoes when a seismic waves passes by (Krebes, 2004). In a continuous and isotropic medium the balance of forces and mass for a very small elemental volume can be expressed as:

$$\rho\ddot{u}_i = \sigma_{ij,j} + f_i \tag{2.1}$$

where $\ddot{u}_i$ is the the second partial derivative with respects to time of the displacement per unit volume of mass or density (ρ), $\sigma_{ij,j}$ is the the stress tensor and f_i corresponds to any additional body forces. Body forces such as gravity can usually be discarded and expression can be written as:

$$\ddot{u}_i = \rho^{-1}\sigma_{ij,j} \tag{2.2}$$

$$\sigma_{ij,j} = C_{ijkl}\partial_l u_k \tag{2.3}$$

where

$\partial_l u_k$ is the strain tensor and C_{ijkl} is the fouth order tensor containing $3^4 = 81$ elastic constants. σ_{ij} and $\partial_i u_j$ are symmetric as seen by $C_{ijkl} = C_{ijlk}$ and $C_{ijlk} = C_{ijkl}$, the number of constants can be reduced to 36 and in an isotropic and continuous medium the number can be reduced to two independent elastic constants:

$$C_{ijkl} = \lambda\delta_{ij}\delta_{kl} + \mu(\delta_{ij}\delta_{kl} + \delta_{il}\delta_{jk}) \tag{2.4}$$

Where μ and λ represents Lame parameters.

At strong reflectors, the boundary conditions of the full wavefield are given. Acoustic waves state continuity at the boundary and the weighted derivatives at the boundary is expressed as,

$$\begin{aligned} p^{(1)} &= p^{(2)} \\ \frac{1}{\rho^{(1)}}\frac{\partial p^{(1)}}{\partial n} &= \frac{1}{\rho^{(2)}}\frac{\partial p^{(2)}}{\partial n} \end{aligned} \tag{2.5}$$

where n is the normal to the reflector into the upper medium and (1) and (2) refers to the layer above and under the reflector. The elastic wave state the continuity of the displacement and corresponding traction vectors at the reflectors:

$$\begin{aligned} p^{(1)} &= p^{(2)} \\ n \cdot T^{(1)} &= n \cdot T^{(2)} \end{aligned} \tag{2.6}$$

These equations form the basics of seismic modelling and the goal of forward seismic modelling is to compute the displacement measured by a set geophones and then to produce a synthetic seismogram. Several different methods or approaches to compute synthetic seismograms exists, common for them all are that they use geological and petrophysical models of the subsur-

face to compute or estimate the wave propagation and resulting seismograms. Each method has it's own advantages and disadvantages and Carcione (2002) categorized them into three main groups,

- Ray-tracing Methods
- Integral-equation Methods
- Direct Methods

Ray-tracing methods are high frequency approximations where the travel times and amplitudes of seismic waves can be calculated using ray paths, these methods are relatively cheap and provide a good results in homogeneous areas (ibid.). Integral-equation methods can be a good approximations in certain specific geometries. Direct methods include finite difference, pseudospectral and finite element approaches which utilizes mesh grids to discretize the time and space variables of the geological model. These methods are sometimes called full-wave equation methods because the full wavefield with all waveforms are calculated and included in the resulting seismogram. The finite difference method using the staggered grid approach is the method used by the seismic modelling software in this study and will be explained more comprehensive in the next section.

2.1.1 Finite Difference Method

Finite difference methods are numerical methods for approximating differential equations by approximating derivatives and they are used to solve a variety of mathematical problems in science and engineering. In this thesis the finite difference approach is used in the seismic modelling of the Madagas-

car software package. The forward difference approximation of the derivative is expressed as:

$$D_+ f = \frac{f(x + \Delta x) - f(x)}{\Delta x} \tag{2.7}$$

here δx represent a finite sized or grid sized step in the x-direction (Krebes, 2004) and the backward and central difference approximations are given by:

$$D_+ f = \frac{f(x) - f(x + \Delta x)}{\Delta x} \tag{2.8}$$

$$D_+ f = \frac{f(x + \Delta x) - f(x - \Delta x)}{2\Delta x} \tag{2.9}$$

the error by using Equation 2.7 and Equation 2.8 are found to be of order Δx whereas the error by using the central difference in Equation 2.9 is found to be of order Δx^2 which shows that as long as Δx is < 1 the central difference will give better results and it is the one used for finite difference modelling in geoscience.

The Madagascar software package includes seismic modelling software based on an explicit approach to solving the differential equations that describe wave propagation in the earth, under a set of initial, final, and boundary conditions similar to the approaches described by Ikelle and Amundsen (2005), Levander (1988) and Graves (1996). It uses numerical approximations of the derivatives of Equation 2.1 in order to simulate elastic wave propagation in the earth and together with complex geological models, produce accurate synthetic seismograms. The explicit approach to finite difference modelling

used in this software is the staggered grid approach where the first-order elastodynamic equations of motion are expressed in terms of velocity and stress (Graves, 1996).

Assuming a three-dimensional, linear and isotropic elastic media Equation 2.2 can be expressed by velocity instead of displacement as:

$$\begin{aligned} \partial_t v_i &= \rho^{-1} \partial_t \sigma_{ij,j} \\ \sigma_{ij,j} &= [\lambda \delta_{ij} \delta_{kl} + \mu(\delta_{il}\delta_{jk})] \partial_l u_k \end{aligned} \tag{2.10}$$

The equations of momentum conservation can now be expressed as:

$$\begin{aligned} \rho \partial_t v_x &= \partial_x \sigma_{xx} + \partial_y \sigma_{xy} + \partial_z \sigma_{xz} \\ \rho \partial_t v_y &= \partial_x \sigma_{xy} + \partial_y \sigma yy + \partial_z \sigma_{yz} \\ \rho \partial_t v_z &= \partial_x \sigma_{xz} + \partial_y \sigma_{yz} + \partial_z \sigma_{zz} \end{aligned} \tag{2.11}$$

The stress and strain relations is expressed as:

$$\begin{aligned} \sigma_{xx} &= (\lambda + 2\mu)\partial_x v_z + \lambda(\partial_y v_y + \partial_z v_z) \\ \sigma_{yy} &= (\lambda + 2\mu)\partial_y v_y + \lambda(\partial_x v_x + \partial_z v_z) \\ \sigma_{zz} &= (\lambda + 2\mu)\partial_z v_z + \lambda(\partial_x v_x + \partial_y v_y) \\ \sigma_{xy} &= \mu(\partial_y v_x + \partial_x v_y) \\ \sigma_{xz} &= \mu(\partial_z v_x + \partial_x v_z) \\ \sigma_{yz} &= \mu(\partial_z v_y + \partial_y v_z) \end{aligned} \tag{2.12}$$

Here (v_x, v_y, v_y) are the components of the velocity vector; $(\sigma_{xx}, \sigma_{yy}, \sigma_{zz}, \sigma_{xy}, \sigma_{xz}, \sigma_{yz})$

are the stress components; ρ is the density; λ and μ are Lame coefficients; and the symbols ∂_x, ∂_y, ∂_z and ∂_{tt} are shorthand representations of the differential operators $\frac{\partial}{\partial x}$, $\frac{\partial}{\partial y}$ and $\frac{\partial}{\partial z}$. It can also be noted that for $\mu = 0$ these equations would represent the acoustic case.

These equations can now be solved recursively with the finite difference method on a staggered time and space grid as seen in Figure 2.2. In Ikelle and Amundsen, 2005 the staggered grid is explained as follows "the shear stresses are defined at the points on the reference grid, whereas the normal stresses, the three components of the particle velocity, the mass density, and the Lamé parameters, are defined as the points half a grid off the reference grid".

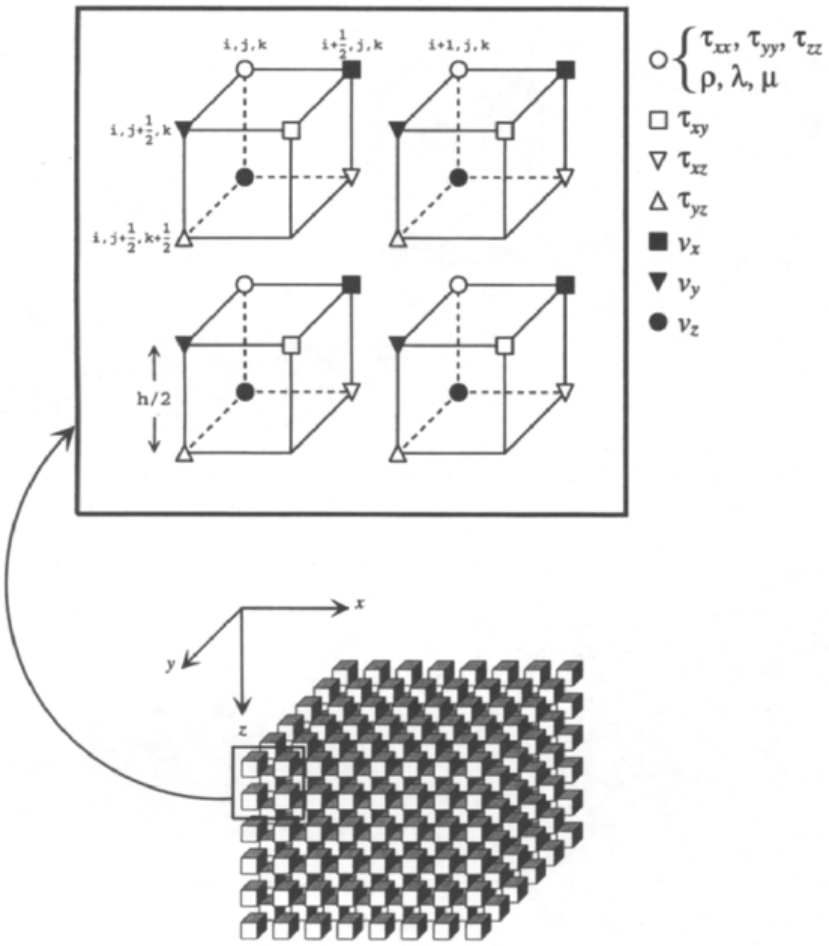

Figure 2.2: The staggered grid for a 3D finite difference model (Graves, 1996)

The discrete form of the first-order differential equations is given by:

$$
\begin{aligned}
v^{n+\frac{1}{2}}_{xi+\frac{1}{2},j,k} &= v^{n-\frac{1}{2}}_{xi+\frac{1}{2},j,k} + \left[\Delta t \bar{b}_x (D_x \tau_{xx} + D_y \tau_{xy} + D_z \tau_{xz} + f_x)\right] |^n_{i+\frac{1}{2},j,k} \\
v^{n+\frac{1}{2}}_{yi,j+\frac{1}{2},k} &= v^{n-\frac{1}{2}}_{yi,j+\frac{1}{2},k} + \left[\Delta t \bar{b}_y (D_x \tau_{xy} + D_y \tau_{yy} + D_z \tau_{yz} + f_y)\right] |^n_{i,j+\frac{1}{2},k} \\
v^{n+\frac{1}{2}}_{yi,j,k+\frac{1}{2}} &= v^{n-\frac{1}{2}}_{yi,j,k+\frac{1}{2}} + \left[\Delta t \bar{b}_z (D_x \tau_{xz} + D_y \tau_{yz} + D_z \tau_{zz} + f_z)\right] |^n_{i,j,k+\frac{1}{2}}
\end{aligned}
\tag{2.13}
$$

for the velocities, and

$$\begin{aligned}
\tau^{n+1}_{xxi,j,k} &= \tau^{n}_{xxi,j,k} + \Delta t[(\lambda+2\mu)D_x v_x + \lambda(D_y v_y + D_z v_z)]\big|^{n+\frac{1}{2}}_{i,j,k} \\
\tau^{n+1}_{yyi,j,k} &= \tau^{n}_{yyi,j,k} + \Delta t[(\lambda+2\mu)D_y v_y + \lambda(D_x v_x + D_z v_z)]\big|^{n+\frac{1}{2}}_{i,j,k} \\
\tau^{n+1}_{zzi,j,k} &= \tau^{n}_{zzi,j,k} + \Delta t[(\lambda+2\mu)D_z v_z + \lambda(D_x v_x + D_y v_y)]\big|^{n+\frac{1}{2}}_{i,j,k} \\
\tau^{n+1}_{xyi+\frac{1}{2},j+\frac{1}{2},k} &= \tau^{n}_{xyi+\frac{1}{2},j+\frac{1}{2},k} + \Delta t[\mu^{-H}_{xy}(D_y y_z + D_x v_y)]\big|^{n+\frac{1}{2}}_{i+\frac{1}{2},j+\frac{1}{2},k} \\
\tau^{n+1}_{xzi+\frac{1}{2},j,k+\frac{1}{2}} &= \tau^{n}_{xzi+\frac{1}{2},j,k+\frac{1}{2}} + \Delta t[\mu^{-H}_{xz}(D_z y_x + D_x v_x)]\big|^{n+\frac{1}{2}}_{i+\frac{1}{2},j,k+\frac{1}{2}} \\
\tau^{n+1}_{yzi,j+\frac{1}{2},k+\frac{1}{2}} &= \tau^{n}_{yzi,j+\frac{1}{2},k+\frac{1}{2}} + \Delta t[\mu^{-H}_{yz}(D_x y_y + D_y v_z)]\big|^{n+\frac{1}{2}}_{i,j+\frac{1}{2},k+\frac{1}{2}}
\end{aligned} \tag{2.14}$$

for the stresses.

Here the discrete form of the differential operators ∂_x, ∂_y, ∂_z and ∂_{tt} are represented by the equations $D_x, D_y, and D_z$. These operators are evaluated by a second- or fourth-order difference which is chosen based on the minimum wavelength in modelling study, where the second-order difference requires a 10 grid points per wavelength and the fourth-order difference requires 5 (Ikelle and Amundsen, 2005; Levander, 1988). The time index is governed by the superscripts and subscripts relate to spatial indices. Therefore using a time step of Δt and grid spacing of h,

$$v^{n+\frac{1}{2}}_{xi+\frac{1}{2},j,k} \tag{2.15}$$

is the x-component of the velocity at $x = [i + (1/2)]h, y = jh, z = kh$ at time $t = [n + (1/2)]\Delta$t as seen in Figure 2.2 (Graves, 1996).

Absorbing boundaries conditions are met by implementing a perfectly matched layer (PML). The idea being that the grid is extended at the edges by placing a viscoelastic medium outside of the original grid. Viscoelastic materials absorb much more energy than the elastic one in the "inner grid" and thereby all waves that travel into the viscoelastic medium is absorbed and not reflected back into the model. In this thesis no free surface is used in order to simplify processing and the top surface is also an absorbing one.

From discussion with Espen B. Raknes it was found that in order to avoid numerical instabilities such aliasing the following conditions had to be fulfilled:

$$\begin{aligned} \frac{C_{max}\Delta t}{\delta x} &\leq \frac{\sqrt{2}}{\pi} \quad (2D) \\ \frac{C_{max}\Delta t}{\delta x} &\leq \frac{2}{\sqrt{3}\pi} \quad (3D) \end{aligned} \tag{2.16}$$

in addition the Nyquist criteria has to be considered as well:

$$f_{max} \leq \frac{C_{min}}{2\Delta x} \tag{2.17}$$

2.2 Forward Seismic Modelling in Geoscience

The following section is taken from previous work by the author in (Steinsbø, 2012). Forward seismic modelling is used widely in geoscience to solve a wide range of problems and in this section some of these problems are presented and discussed. A forward seismic modelling work flow is presented and some case studies from literature is studied.

2.2.1 Motivation

There are several motivations for doing forward seismic modelling and some of the most prominent are:

- To test data processing algorithms
- To compare modeled data with measured data
- To better understand seismic wave propagation
- To design acquisition parameters in survey planning

Forward seismic modelling can often be a good tool for testing processing or migration algorithms. It can be thought of as an extrapolation of the wavefield through a geological model from the source to receiver in order to generate a synthetic seismic section. Migration on the other hand can be seen a process where the signal at the receivers are extrapolated backwards towards the source in order to generate a seismic image of the subsurface. Forward seismic modelling can therefore be viewed as the opposite of a migration and it therefore be a good method for testing how accurate a migration

or processing algorithm is (Yilmaz, 2001).

Comparing modelled data with acquired data from the field is a common motivation for doing forward seismic modelling. An example is that forward seismic modelling can be a tool for verifying seismic interpretations. A geological model based on the interpretation can be produced and the resulting synthetic seismic can be matched with the real seismic. Changes can be made to the model if significant differences are found. Models can also be produced to test different geological interpretations with variations in lithology and fluid content. Geological and geophysical phenomena such as thin layers, tuning effects, complex structures and direct hydrocarbon indicators can be also modeled. Updating the geological model based on results from seismic modelling is an important step of this method.

Full-wave form modelling approaches can be used to better understand seismic wave propagation especially concerning complex geological structures, salts etc (Tøndel, 1997). Forward seismic modelling is also used to design the acquisition parameters, simulated surveys using seismic modelling are used to test different acquisition parameters and geometries to find the optimal data collection strategy.

2.2.2 Geological model

There are several methods or approaches that can be taken when doing forward seismic modelling, aside from various numercial algorithms for modelling wave propagation discussed in the previous section, and they differ in what kind of input is used in the geological model and how the model is

made. Different types of input can be:

- Seismic section(s)
- Well data and core samples
- Geological outcrops
- Synthetic model
- Combination of these

Interpreted seismic sections either from a 2D or a 3D survey can be used as inputs for geological models used in forward seismic modelling. Velocities and densities can be acquired from well logs and/or core samples and an acoustic impedance model can be produced. Stratigraphic models can be made based on well data and for inversion and processing purposes a simple synthetic model can be used to test algorithms. During fieldwork, outcrops can be interpreted, and geological models can be made based on these interpretations, Johansen, Kibsgaard, et al. (1994) show an excellent example of this method from Svalbard. The best method is perhaps to combine two or more of these methods, as more data will result in a better and more comprehensive geological model. One example is that interpreted seismic sections can represent the structural part of a model whereas well data and core samples can be used to determine the rock properties in the model.

2.2.3 Forward Seismic Modelling Work flow

A work flow for performing forward seismic modelling can be divided into several steps:

1. Interpreting Input Data
2. Build a Geological/Structural Model
3. Set Geometry and Grid Size
4. Assign Rock Properties
5. Export and Import Model/Grid
6. Model Synthetic Seismic
7. Process Synthetic Seismic
8. Correlate Synthetic Data with Real Data
9. Update Geological Model According to Correlation

The first step is to interpret the input data and produce a geological interpretation which will serve as a basis for a geological model. Building the geological or structural model based on the geological interpretation is the next step in the work flow. Setting a geometry and grid size are the following steps and one should take care to set an appropriate geometry. It should be large enough to include all desired events but it is important to note that a larger model will result in longer computation time. The grid size is set on basis of the geometry, the modelling approach used, desired quality of the resulting seismograms and computation power available. Usually the interpretation has to be modified to fit into the chosen grid and some of the detail is lost in the translation from interpretation to geological model. Once a satisfactory geological model has been made rock properties are added to the model depending on lithology and fluid content in porous rocks. This

data can be gathered from well logs, core samples, cuttings or rock samples and from estimations using rock physics models. The next step now is to perform the seismic modelling and then, depending on the output seismic data processing may be appropriate. For asymptotic methods which produce a perfectly migrated image this is unnecessary but for full-wave form methods noise and multiples has to be removed and the sections have to be migrated. Once a satisfactory image has been produced it can be compared with the real data and the differences between the two can be evaluated. If significant discrepancies are found the geological model has to be altered and than the process repeated iteratively until a satisfactory results is found.

2.3 Seismic Imaging

This sections aims to give a short presentation of the seismic imaging principle and give a short introduction to the two migrations which will be used in this thesis, Kirchoff Pre-stack time migration and reverse time migration.

The idea behind seismic imaging or migration is to make an image of subsurface from seismic data. This is can be achieved by simply preforming a cross correlation between the downwards (D) and upwards (U) propagating wavefront seen in Figure 2.3. At the time of the reflection they will coincide at R (Arntsen, 2013). The reflectivity R(x) is then given as:

$$R(x) = \int dt U(x,t) D(x,t) \tag{2.18}$$

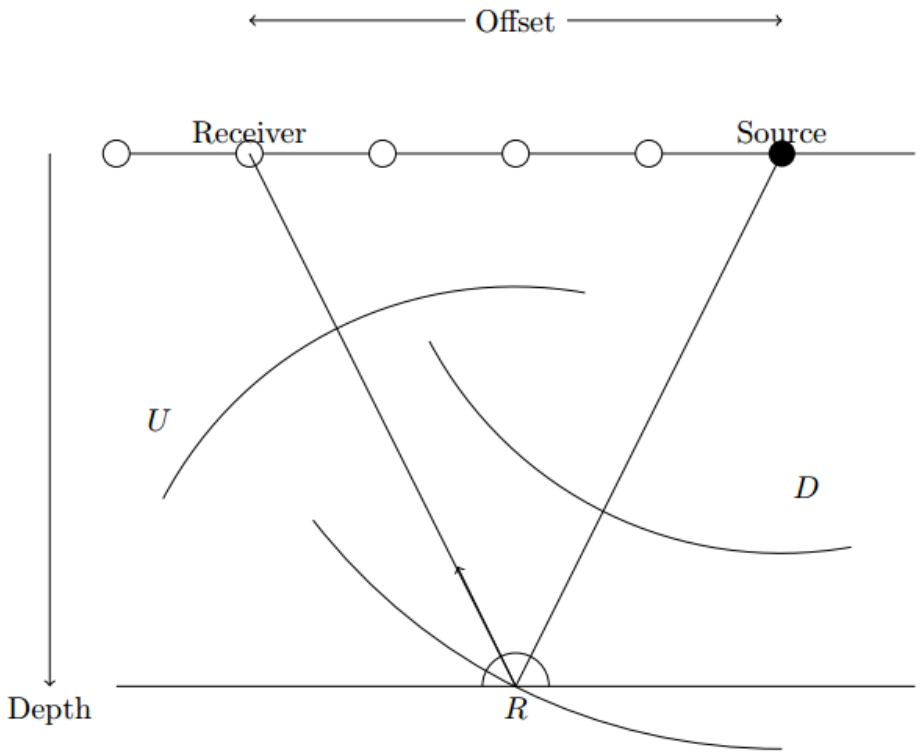

Figure 2.3: Sketch of the imaging principle with a downwards propagating and upwards propagating wavefront coinciding at the reflection point R taken from lecture material by Børge Arntsen (2013)

2.3.1 Kirchoff Time Migration

The up- and downgoing wavefields have to known in order to compute the reflectivity and ray approximations are one way to compute them

$$\begin{aligned} D(x,t) &= A\delta(t-\tau_s) \\ U(x,t) &= BP(t-\tau_r) \end{aligned} \tag{2.19}$$

where A and B are amplitude factors, P is the recorded data, τ_s is the travel-time from source to reflection point and τ_r is the travel-time from reflection point to receiver (Arntsen, 2013). Equation 2.19 and Equation 2.18 can then be put together and integrated and by disregarding the amplitude factors AB one is left with $R(x) = P(\tau_s + \tau_r) = P\tau$ representing the imaging of point x. It is importnat that many source -receiver pairs will contribute to imaging the same point in the subsurface.

By assuming that the velocity only changes with depth one can approximate the travel times as follows,

$$\begin{aligned} \tau_s &= \sqrt{\frac{(x - x_s)^2 + (y - y_s)^2}{c^2} + \tau_0^2} \\ \tau_r &= \sqrt{\frac{(x - x_r)^2 + (y - y_r)^2}{c^2} + \tau_0^2} \end{aligned} \tag{2.20}$$

where c is the velocity, (x_s, y_s) is the source location, (x_r, y_r) is the receiver location and τ_0^2 is the vertical travel time (ibid.). The velocity model used for Kirchoff time migration has to be very smooth and therefore not image lateral changes in velocity as well.

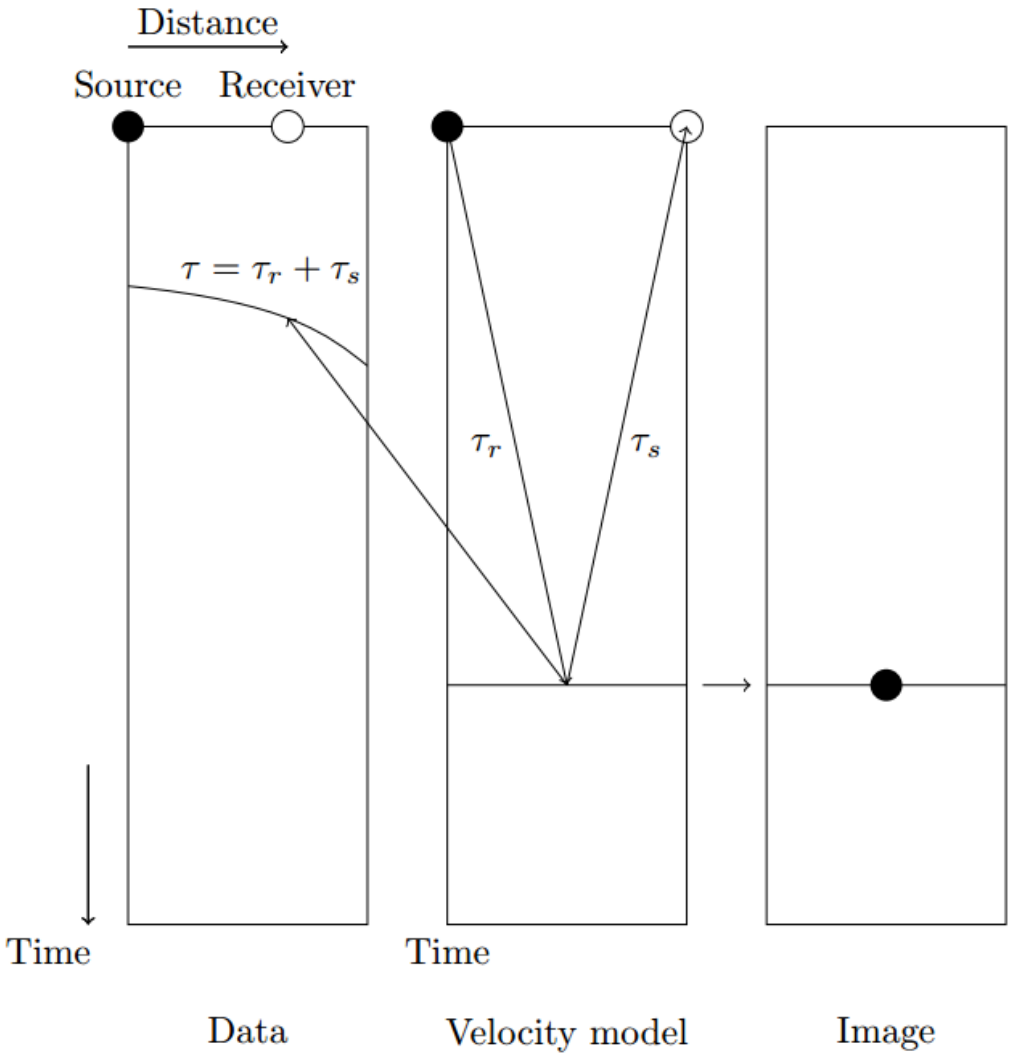

Figure 2.4: Sketch of the principle behind Kirchoff time migration where a only depth dependent velocity model is used to image the reflection point from a source-receiver pair taken from lecture material by Børge Arntsen (2013)

2.3.2 Reverse Time Migration

Reverse time migration is alternative way to compute the up- and downgoing wavefields by solving the elastic wave equation through finite difference

methods as discussed earlier in this chapter. This is done by solving the wave equation with the time reversed and basically going backwards in time from the receivers. This wavefield can then be cross correlated with a forward propagating wavefield from the source. This method is a depth migration and requires more a detailed velocity model but will give better images in areas with significant changes in lateral velocity.

Chapter 3

Geological Setting

Exposed outcrops of collapsed Mesozoic strata and associated infill deposits found at Kvalvågen on the east coast of Spitsbergen as seen in Figure 3.1. The collapse and infill structures are buried by layers of alternating sand and shale. This outcrop is well studied and publications by Nemec et al. (1988b), Nemec et al. (1988a) and Onderdonk and Midtkandal (2010) have studied the area closely with regards to the depositional envirnoment and the mechanisms behind the collapse event. This section will summarize some of the information found in literature regarding the geological setting of both South East Svalbard in general and the study site especially.

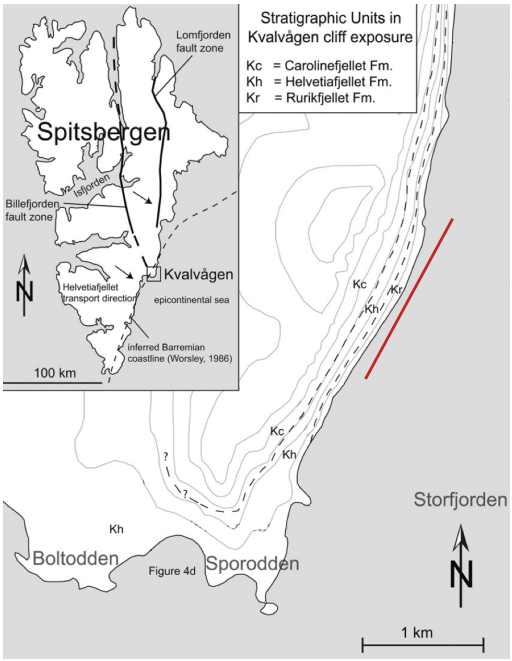

Figure 3.1: This Map modified from Onderdonk and Midtkandal (2010) of the study site at Kvalvågen with the red line representing the outcrop. The smaller map in the upper left corner illustrates Kvalvågens location on Svalbard as well as the inferred coastline during the Early Cretaceous and transport direction of the Helvetiafjellet Formation (Worsley and Aga, 1986)

3.1 Stratigraphic Setting

The stratigraphy at Kvalvågen consists of clastic sediments deposited on a low-gradient shelf in the shallow epicontinental Boreal basin during the Early Cretaceous, and occurrences decreasing sea level has resulted in deposition of sand in an otherwise mud dominated basin. Figure 3.2 shows the stratigraphic column found at the outcrop and it consists of the upper Rurikfjellet Formation, the Helvetiafjellet Formation and the lower Carolinefjellet Formation.

3.1.1 Rurikfjellet Formation

The Rurikfjellet Formation is the oldest formation recognized in the outcrop at Kvalvågen, with only the upper part of the formation exposed in the present day outcrop. Generally the Rurikfjellet formation on Spitsbergen is interpreted to be deposited on a regressive open marine shelf and Onderdonk and Midtkandal (2010) found the exposed strata at Kvalvågen to contain five upward coarsening parasequences dominated by clay-rich mudstone but sandstone is also recognized in the section.

The contact with overlying Helvetiafjellet Formation is an erosive one and is attributed to a regional subaerial unconformity formed by a relative fall in sea level in the epicontinental sea (Midtkandal and Nystuen, 2009)

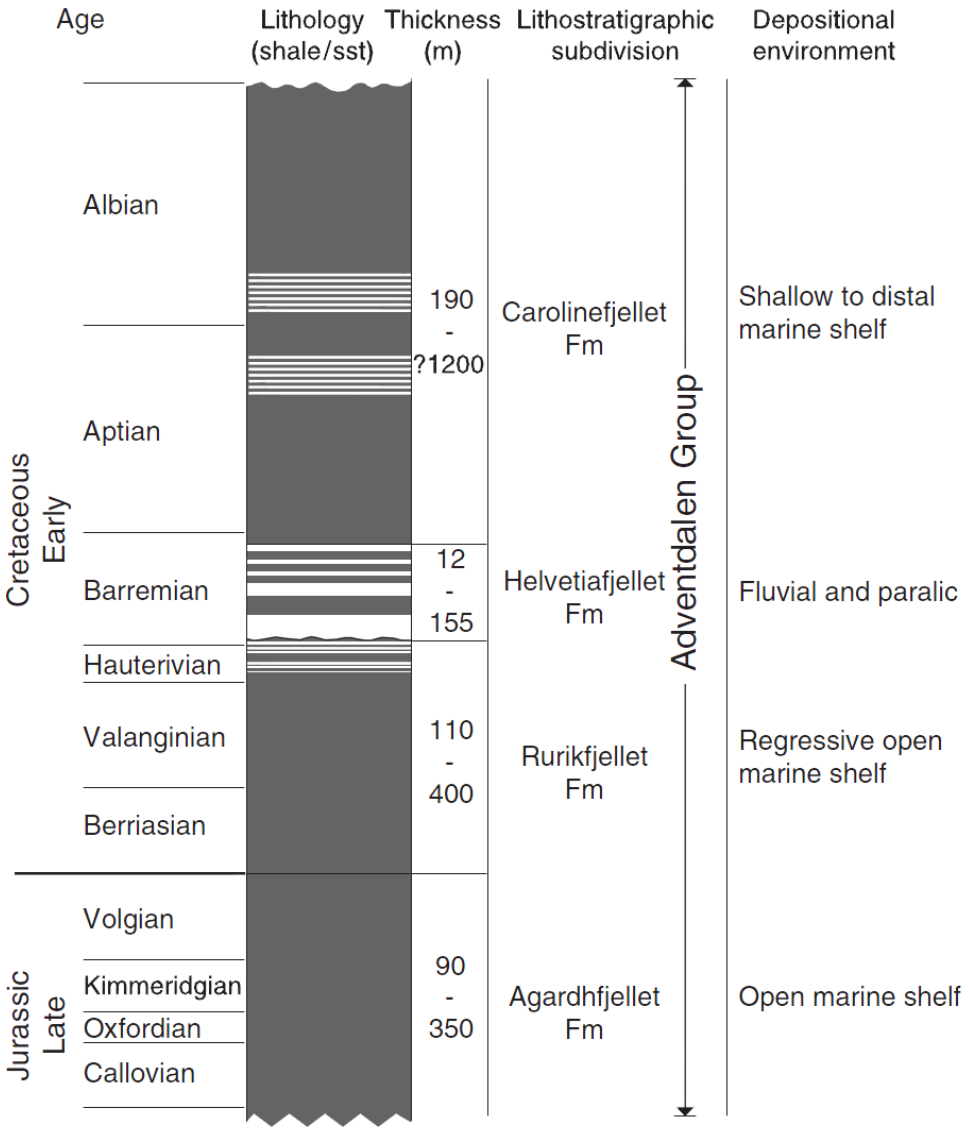

Figure 3.2: The Late Jurassic to Early Cretaceous stratigraphy of Svalbard expropriated from Onderdonk and Midtkandal (2010) in Mørk et al. (1999)

3.1.2 Helvetiafjellet Formation

The lower Cretaceous Helvetiafjellet Formation in Eastern Spitsbergen is a predominantly sandstone succession deposited as a fluvial to coastal plain and paralic unit (Midtkandal and Nystuen, 2009). In Kvalvågen the lowest part part of the Helvetiafjellet Formation are the rotated fault blocks of the Festningen sandstone member, a 20 m thick sandstone unit resting on top of the Rurikfjellet Formation where most of the unit has slid sown and roatated during the collapse. There is some debate in the literature regarding the Festsningen member, whether it represents braided fluvial channel deposits (Onderdonk and Midtkandal, 2010) or it is the distributary channel of a prograding delta (Nemec et al., 1988a,b), and in this study the braided fluvial channel deposits is the favoured interpretation. A 2-4 m thick unit of inter bedded sand and siltstones are recognized both on the faulted blocks and the undisturbed section which (Onderdonk and Midtkandal, 2010) interpreted as coastal floodplain deposits.

Slumps and mass flows of sediments from the Rurikfjellet Formation is thought to represent the initial infill of the collapsed area and is overlain by the main infill made up of turbidites and sandier debris flows (Nemec et al., 1988a).

Following the collapse event in Kvalvågen and subsequent infill deposition a marine transgression occurred and led to an aggradational development of coastal plain and paralic depositional environments (Midtkandal and Nystuen, 2009). Delta mouth bars are recognized at Kvalvågen and thought to represent either a prograding delta front or delta lobe and delta plain and Coastal plain deposits are interpreted on top of the delta mouth bars (Onderdonk

and Midtkandal, 2010). A marine flooding is recognized in the area at the onset of the shale dominated Carolinefjellet Formation.

3.2 Structural Setting

The main structural features recognized at the Kvalvågen outcrop are all a result of the collapse event which occurred as the Helvetiafjellet formation was being deposited. Large blocks slid down and rotated into their present day positions in underlying strata and was followed by infill of smaller blocks, slumps and turbidites. Minor faults and lithological discontinuities are also identified in the outcrop (Onderdonk and Midtkandal, 2010). There was most likely been a fair amount of erosion after the collapse and in the present day the largest slide blocks are roughly 10-20 meters high. Several theories about the collapse is postulated in the literature but this is not the topic of this thesis.

Chapter 4

Dataset

The data used in this thesis are based on unplublished work by S. E. Johansen and R. Mittet and O. Fjeld and R. Tøndel from 1999 and contains an image of the Kvalvågen outcrop and measurments of rock samples taken at the outcrop. The picture of the outcrop is taken from the front and some of the curvature of the outcrop is not as prominent and it is treated as 2D image in this thesis and the curvature is not taken into account. The image is found in Figure 4.1.

Figure 4.1: Picture of the outcrop at Kvalvågen which is used in this study to interpret the geological setting at Kvalvågen and building a geological model.

Chapter 5

Methods

This chapter aims to discuss the methods and software used in this thesis and how they are used to produce the results of the thesis. The Petrel software was used to build the geological and petrophysical models of this thesis while the Madagascar software package was used to in the forward seismic modelling and seismic processing part of the study.

5.1 Petrel

This section will cover how the Petrel software has been utilized to build geological and petrophysical models based on the interpretations of the field data. Petrel is a versatile software developed by Sclumberger and is used in all aspects of the life of an oil field from exploration to reservoir modelling and simulation. Building a geological model is a crucial step in seismic modelling as several important decisions taken during this process will greatly influence the computation time of the seismic modelling and processing and they will factor heavily in the quality of the end product. In this study care has been taken to build a model with a small grid as the goal is to investigate reflection from thin layers.

Petrel is used to build geological and petrophysical models of a field outcrop using a picture of the outcrop and petrophyscial measurements from field samples. Petrel is used in the oil and gas industry to build geological models which are most often used in reservoir simulation and no examples of using Petrel models in seismic modelling was found in literature. Three separate methods for building 3D models exists in Petrel, Make simple grid ,Corner point gridding and Structural framework where the two latter ones use faults that run through the entire model as pillars in the grid framework. This automatically excludes them for use in this study as the seismic modelling software has to have a regular grid as input. The Make simple grid process which uses surfaces as input is left as the preferred method for building models in this study.

The model was created from a model sketch which is imported into the soft-

ware and assigned an appropriate geometry after which surfaces are created based on the model sketch. After all the horizons or surfaces are made a regular grid is made from two flat surfaces and the geological and petrophysical models are produced by assigning properties between the surfaces. The last step was to export the models in an Eclipse format so that they could be imported in the seismic modelling software.

A more step by step explanation of how the models were made is found in Appendix B.

5.2 Madagascar

This section will cover how synthetic seismic data was acquired and processed using the Madgascar sotware package in this thesis.

Madagascar is an open-source software package for multidimensional data analysis and reproducible computational experiments and it is used in this study to perform seismic modelling and seismic processing. The package is made up of several software packages designed to perform specific tasks which all work with a common file format called the Regularly Sampled Format (RSF). This format is simpler and easier to manage then the SEG-Y format used in conventional seismics. The software construction tool Scons is used in Madagascar to manage and reproduce computional experiments and processing flows through python based scripts.

Most of the programs used to do seismic modelling and processing in this thesis are written by Espen B. Raknes and Børge Arntsen of NTNU and can be found for free on Madagascar's homepage www.reproducibility.org.

Madagascar operates on UNIX commands and is a fairly simple environment to handle after some practice. Executing a command is done by calling a program and choosing which files to read to and from as such:

program < file1.rsf key=value > file2.rsf

Several progrmas can be linked together through piping in Madagascar as such:

program1 < file1.rsf | program2 key=value1 | program3 key=value2 > file2.rsf

A more in depth explanation of some of the most used programs and walk though of how to do simple seismic modelling is given in C.

Scons scripts makes Madagascar much more flexible and fast to work with as several programs can be run together in order to increase productivity and make jobs easily reproducible. The scripting command used in this thesis were Flow and Result which have the following syntax:

Flow(file2, file2, program)
Result(file2, plotting program)

All of the SCons scripts used in this thesis can be found in Appendix A.

5.2.1 Modelling on cluster nodes

The Kongull cluster is used in the seismic acquisition part of this thesis because seismic modeling is a computationally expensive method and the use of cluster nodes significantly speeds up the process. The seismic acqusition is run in parallell so that every shot can be simulated at the same time on different processors on the cluster.

Chapter 6

Results

6.1 Geological Interpretation

The geological interpretation of the outcrop at Kvalvågen as seen in Figure 4.1, is based on the aforementioned picture, the field samples collected by Ståle Johansen et. al in 1999 and previous studies of the area as discussed in chapter 3. The geological interpretation will be used to make a geological and petrophysical models for forward seismic modelling

Faulted structures in the lower part of the section are the most prominent features of the section and faulted strata is interpreted to be the mud dominated Rurikfjellet Formation with the fluvial Festningen member sandstone deposited on top. Half grabens and topographic depressions were formed as a result of the collapse and was filled initially with slumps and debris flows followed by turbidites and sand flows deposits (Nemec et al., 1988a). Several large blocks from the Festningen member sandstone member, some of which are heavily rotated, have slid down as a result of the collapse and are

recognized as parts of the infill strata. After a period of of sea level rise and erosion following the collapse event a delta started to prograde across the south eastern part of Spitsbergen and delta mouth bars are interpreted on top of the infill sediments. Depressions both on the south and north side of the outcrop are filled to a greater extent by the mouth bar sediments then the horst structures at the center of the outcrop. Thicker packages of alternating sand and shale is interpreted as delta top sediments and the Carolinefjellet Formation is interpreted a the top of the section more dominated by silt- and mudstones. Figure 6.1 (a) presents the interpretation of the outcrop at Kvalvågen and show the various formations or depositional environment.

Based on the interpretation shown in Figure 6.1 (a), a detailed geological model of the outcrop is made by placing a sheet of natural tracing paper on top of the picture in Figure 4.1 and making a detailed lithological interpretation as seen in Figure 6.1 (b).

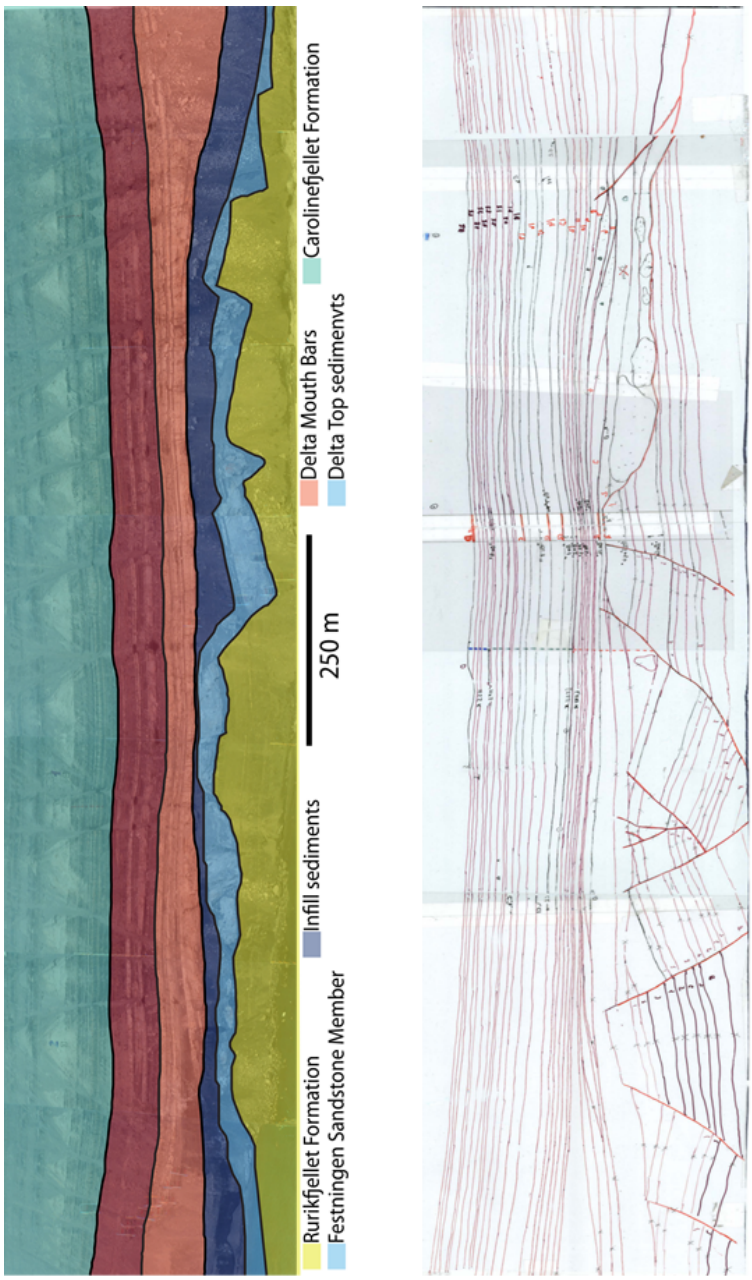

Figure 6.1: Interpretation of the outcrop at Kvalvågen where figure (a) is an interpretation of the various formations and sedimentary depositional environments found at Kvalvågen and (b) is a more in depth lithological interpretation made with natural tracing paper.

6.1.1 Model Building

Following the workflow presented in section 2.2 for creating geological models in Petrel, the tracing paper lithological model in Figure 6.1 (b) was imported and the resulting lithological model made in Petrel can be seen in Figure 6.2. The outcrop at Kvalvågen is a three dimensional object. However the picture of the outcrop used in this study is two dimensional, and therefore the model is not a true representation of the outcrop as some of the depth and curvature of the outcrop is lost in the process. In order to acquire a complex and realistic seismic section a detailed lithological model is required, and this is why the model seen in Figure 6.2 contains a lot of layers, some of which are only a couple of meters thick, to produce a result that is as realistic and of the highest quality possible.

After the geological model is built the next step of the workflow found in section 2.2 is to determine the grid size and geometry. As discussed in section 2.2 the grid size has a big effect on computational time and quality of the final image. The outcrop at Kvalvågen is of a reservoir scale with a length of 1500 meters and hight of approximately 250 meters and therefore it is possible to make a fine and detailed model of the outcrop. A grid size of 1m x 1m x 1m was chose for this study so that the model would be as accurate as possible. The model is made as a three dimensional model in Petrel, however the third dimension (depth) is non changing due to lack of data, and the model can be referred to as a 2.5D model.

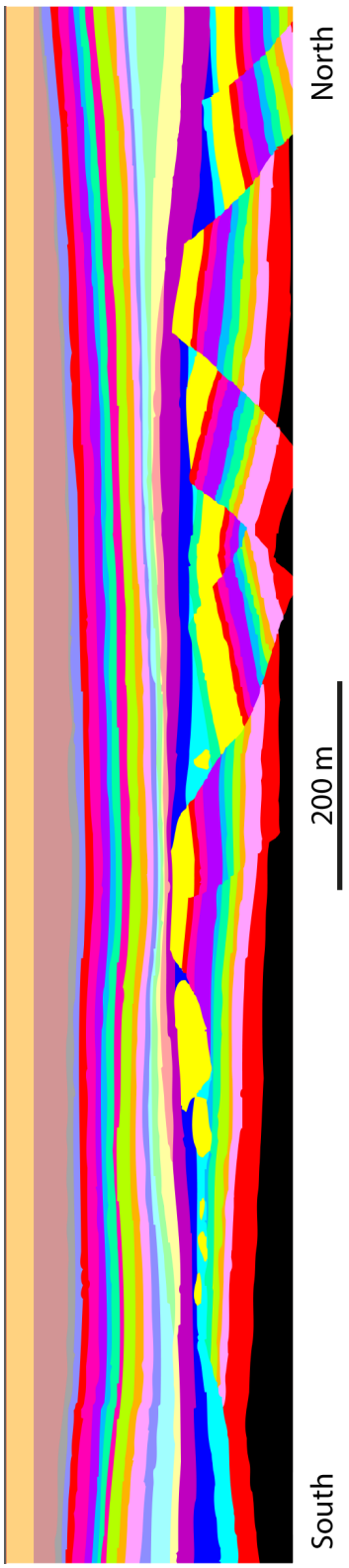

Figure 6.2: Structural model of the Kvalvågen outcrop created from the image seen in Figure 6.1 (b) in Petrel.

6.1.2 Petrophysical Properties

Once the structural model of the outcrop was completed, the next goal was to populate the model with the velocity and density data that is needed to simulate wave propagation thorough the model. Laboratory measurements on rock samples found in Table 6.1 are taken at the outcrop and form the basis for the rock properties used in this study. These measurements have been correlated with data from a nearby well log and compared with numerical relationships between rock properties. The rocks at Kvalvågen have been buried to great depths and have after erosion been exposed to wind and weather which will lead to rock cementation and subsequently result in higher measured velocities. Some of the values in Table 6.1

Sample Number	Vp	Vs	ρ
1	2.46	1.58	2.41
2	3.3	2.22	2.57
3	2.95	1.92	2.55
4	2.58	1.96	2.51
5	2.77	1.87	2.51
6	3.29	2.16	2.56
7	4.4	2.86	3.1
8	2.65	1.86	2.52
9	5.0	3.19	
10	2.33	1.77	2.63
11	3.23	2.24	2.55
12	2.6	1.79	2.44
13	2.39	1.72	2.45

Table 6.1: Velocity and density data from rock samples collected in the Field by Ståle Johansen et. al in 1999 where Figure 6.3 indicate where the rock samples are taken on the outcrop.

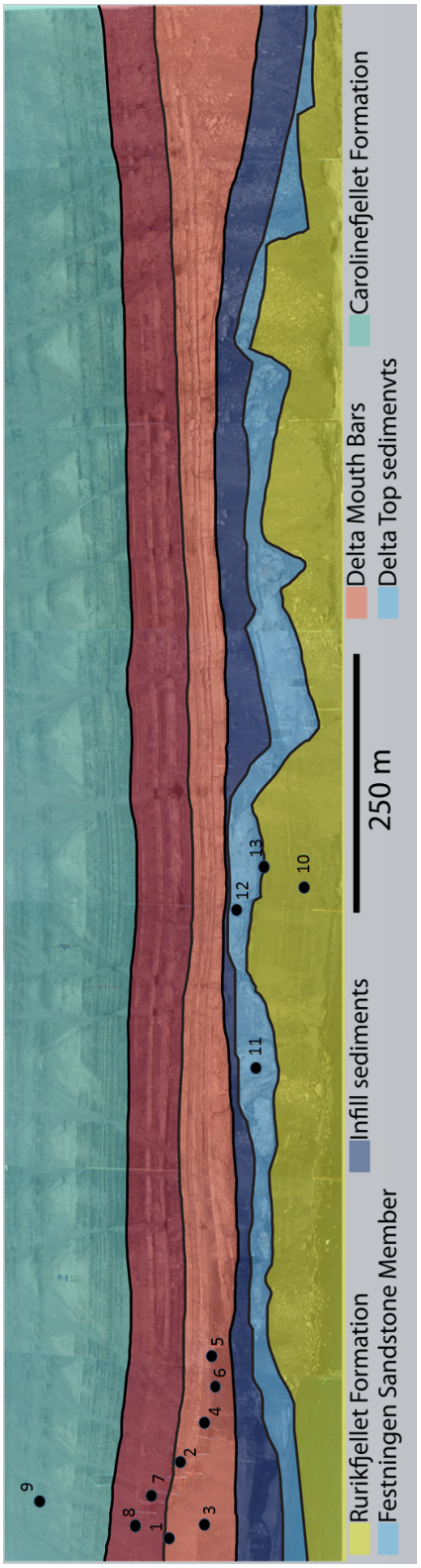

Figure 6.3: Illutstration of where on the outcrop the samples found in Table 6.1 are taken from

The method used in this thesis to build the property models was to first define a empty grid with the desired geometry and grid size and then afterwards use surfaces to populate the model by assigning property values between two surfaces. The property models as seen in the Petrel software can be found in Appendix B.

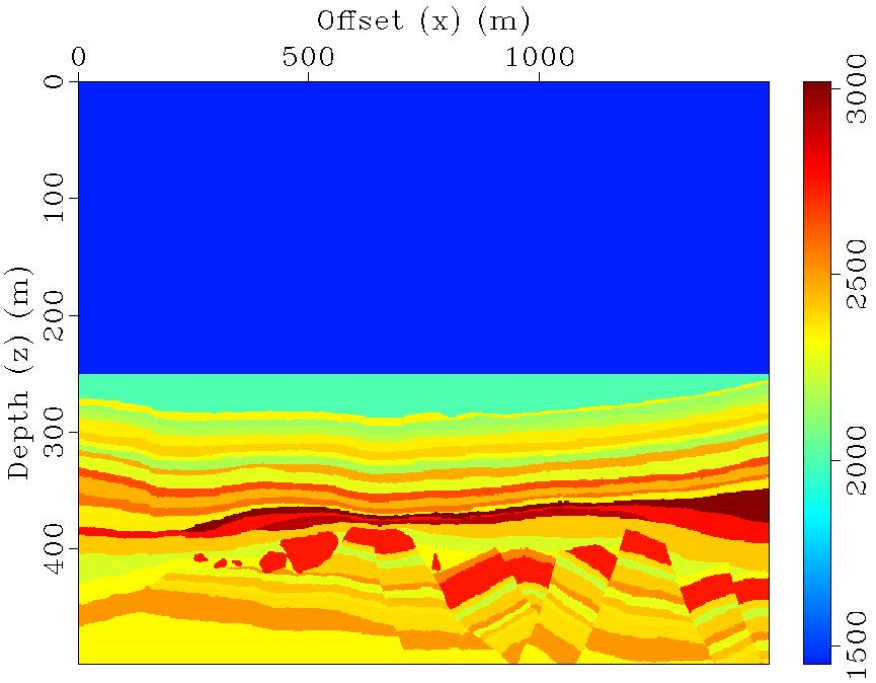

Figure 6.4: P-wave velocity model

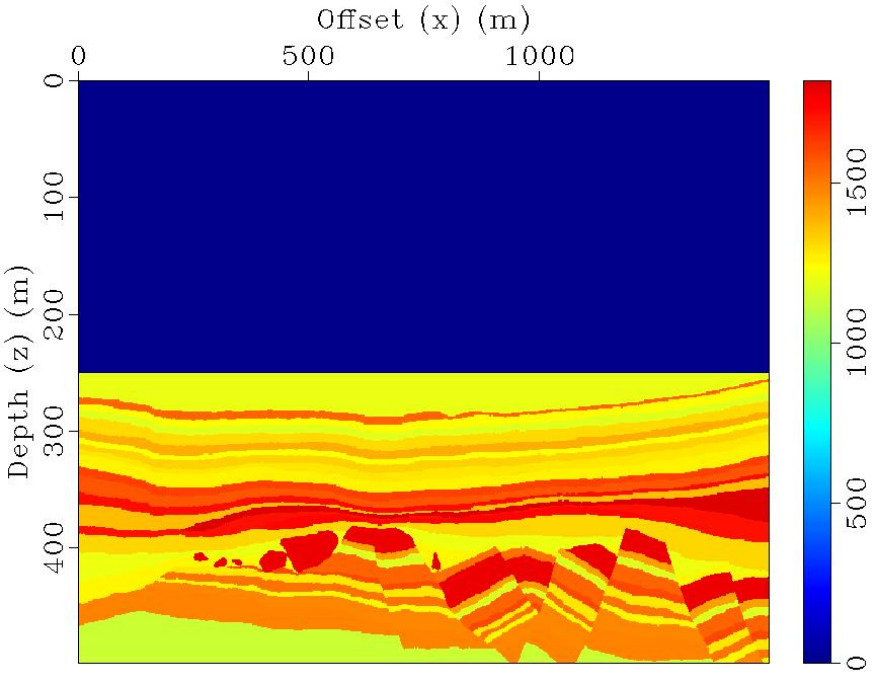

Figure 6.5: S-wave velocity model

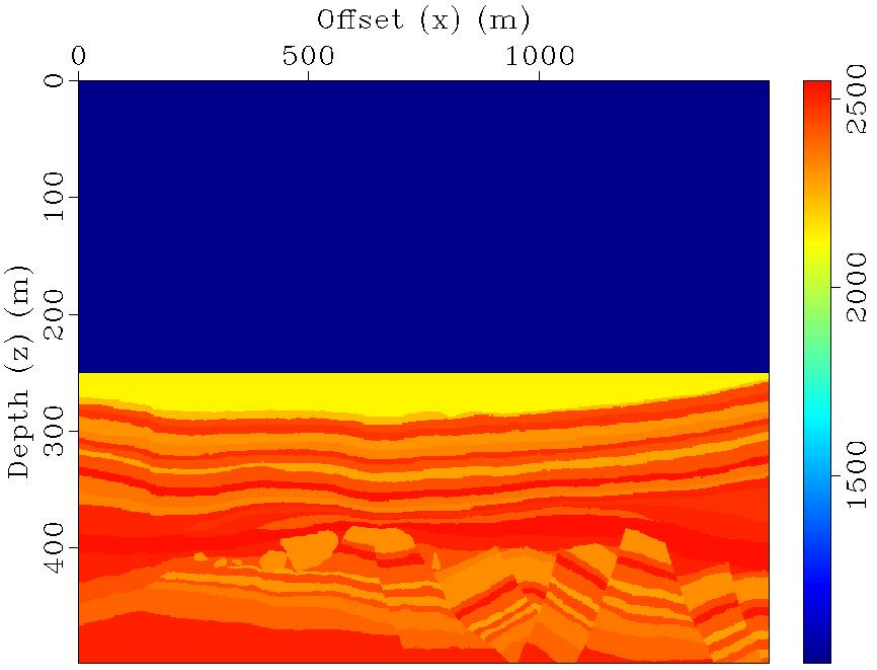

Figure 6.6: Density model

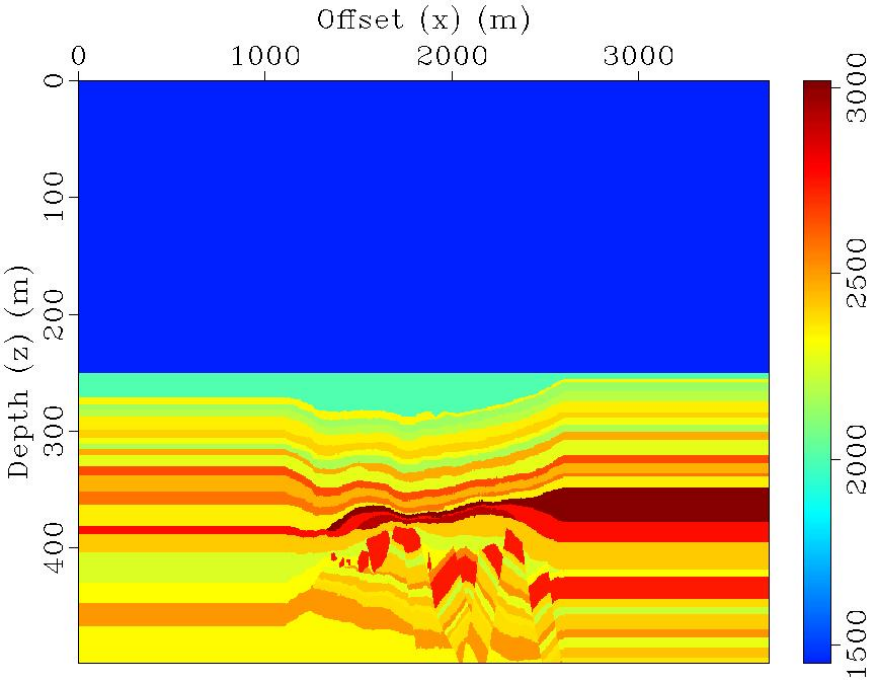

Figure 6.7: P-wave velocity model spanned for acquisition

6.2 Seismic modeling

Seismic modelling experiments performed in this thesis is presented in this section.

6.2.1 Acquisition parameters

The acquisition set up and geometry was used for most experiments in this thesis can be found in Table 6.2 and Figure 6.8. Local models were used in the parallel modelling to decrease the computation time by modelling over smaller models and all models were spanned out 1100 meters on both ends

to acquire a high fold. Considering the shallow geological model a relative short cable of 1000 m was assumed sufficient to acquire enough data to image the section. The local models were set to be 1100 m long, the shot spacing 10 m and receiver spacing 4 m which resulted in a maximum fold of 200. The shot was placed 100 m inside the local models to minimize numerical noise from the model boundary. The start of first local model is located 1100 meters from the actual geological model and the first shot is placed 1 km from the geological model while the last shot is placed at the end of the geological model. The distance between the first and last shot is 2600 m and consequently 260 shots were shot in the acquisition. A ricker wavelet with a center frequency of 100 Hz was used as source in the modelling. The free surface was not used in any of the experiments in order to avoid multiples in the processing.

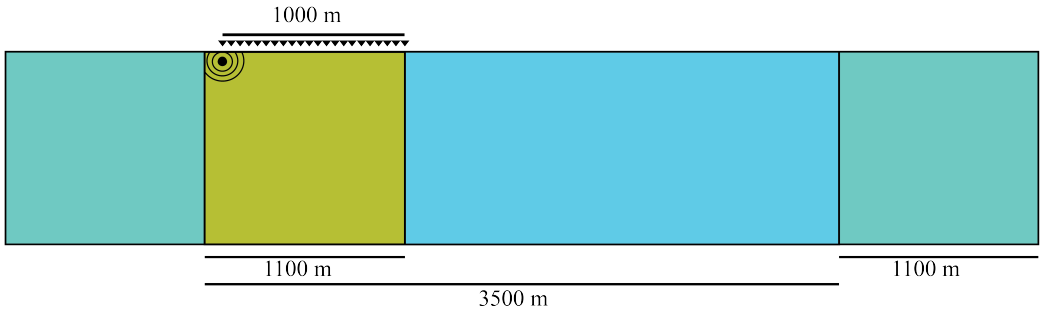

Figure 6.8: Illustration of acquisition geometry and acquisition method used in the experiments in this thesis. The green boxes at the sides represent padding of 1100 m added to the models in order to acquire data with high fold over the entire model. The dark yellow box demonstrate a 1100 m long local model, local models are used in the acquisition process to minimize computation time. Each shot is located 100 m inside the local model to avoid to much numerical noise from the model boundary.

Parameters	
Number of shots	260 m
Number of receivers	250
Shot spacing	10 m
Receiver spacing	4 m
Source depth	3 m
Receiver depth	6 m
Cable length	1000 m
Max fold	200
Peak frequency of Ricker wavelet	100 Hz
Recording time	1 s

Table 6.2: Table of the various parameters used in acqusition of synthetic seismic data.

6.2.2 Seismic modelling of a single shot

A seismic modelling experiment with a single source was tested so that in-depth examinations of the wavefield and wave propagation could be performed. The shot #130 was chosen and it covers some of the of the interesting features in the model. The local model for shot #130 is located 1300 m inside the spanned model found in Figure 6.7 and the acquisition parameters used in this experiment was identical to the ones listed in Table 6.2.

As discussed in chapter 2 the seismic modelling computes the normal stress, shear stress and particle velocity of the entire model for each time step and the wave propagation can be studied by extracting the vertical component of the normal stress for certain time steps. In this thesis the P-wave velocity model for shot #130 (Figure 6.9) was put on top of top of the wave field to better understand the various wave phenomena observed.

Figure 6.10 exhibits the wavefield at 0.21 seconds and a couple of interesting observations are made. As the free surface set to give no reflection the ghost

reflection usually found in seismic data is not present here. The 'A' is placed next to the ocean bottom reflection headed back up towards free surface. Less than marginal numerical noise was observed near the model boundaries at this time step. 'B' is placed where the first reflection below the sea bottom occurs. In Figure 6.11 the wavefield is moved forwards to 0.23 seconds and the 'A' still indicates the seabottom reflection. 'B' indicates the first reflections travelling up and into the water layer with one event reflected back down from the seabottom as an inner bed multiple. 'C' is placed between the pressure wave and the converted S-wave which has a lower velocity.

Figure 6.12 display the wavefield at 0.28 seconds with 'A' indicating reflections traveling back up towards the receivers below the ocean surface. Several wavefronts of converted S-waves can be identified in this image near 'B'. At 'C' several diffractions are identified after the wavefront has passed through the smaller fault blocks in the model. It is also noted how the wavefront thickens in deeper parts of the model containing higher velocities. This thickening gives a lower seismic resolution. At 0.36 seconds the wave has passed through the entire model at offsets up to around 300 meters as seen in Figure 6.13. 'A' indicates the reflection from the sea bottom which is almost at the receivers. A weak reflections from the model boundary is observed just left of the 'A'. The wavefront is observed just in front of 'B' and the two converted S-waves is identified just behind it.

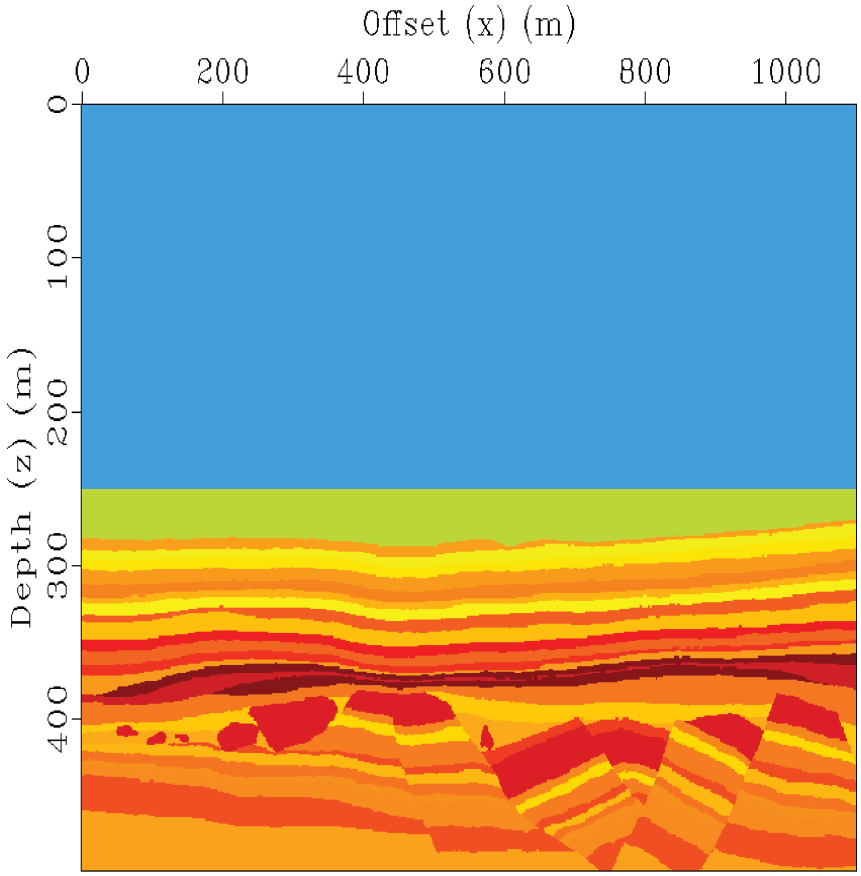

Figure 6.9: The P-wave velocity model for local model #130 which show the extent of local model #130. The velocity model is also used in subsusequent figures with the wavefield in this section.

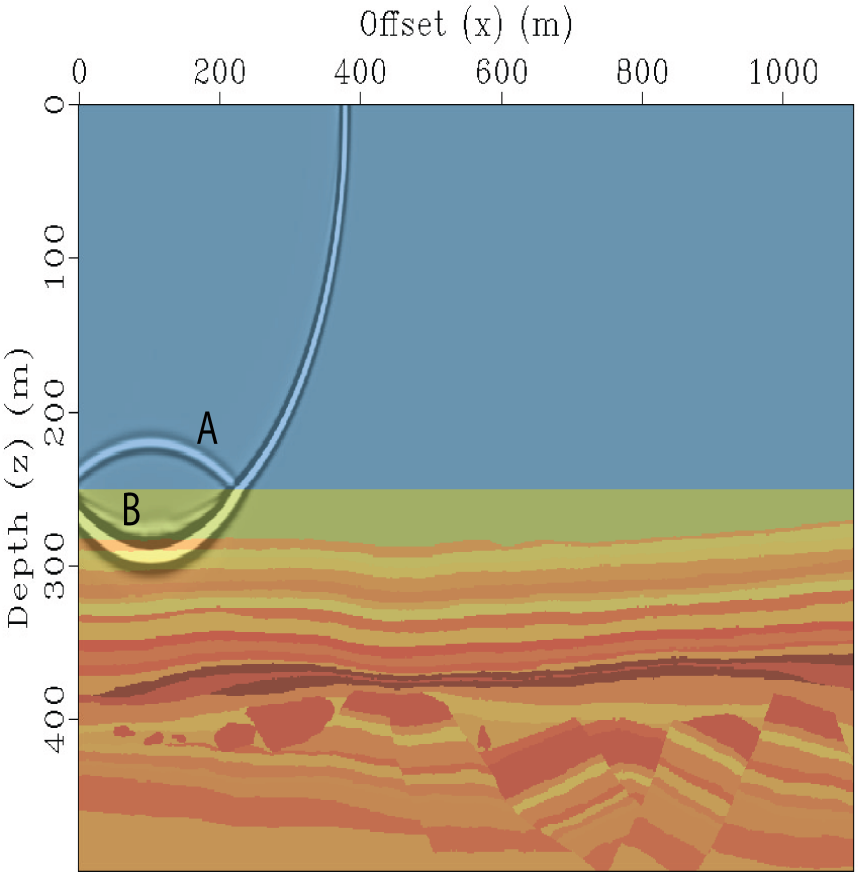

Figure 6.10: Time snap of the wavefield for shot #130 at time 0.21 seconds overlain by the P-wave velocity model for local model #130.

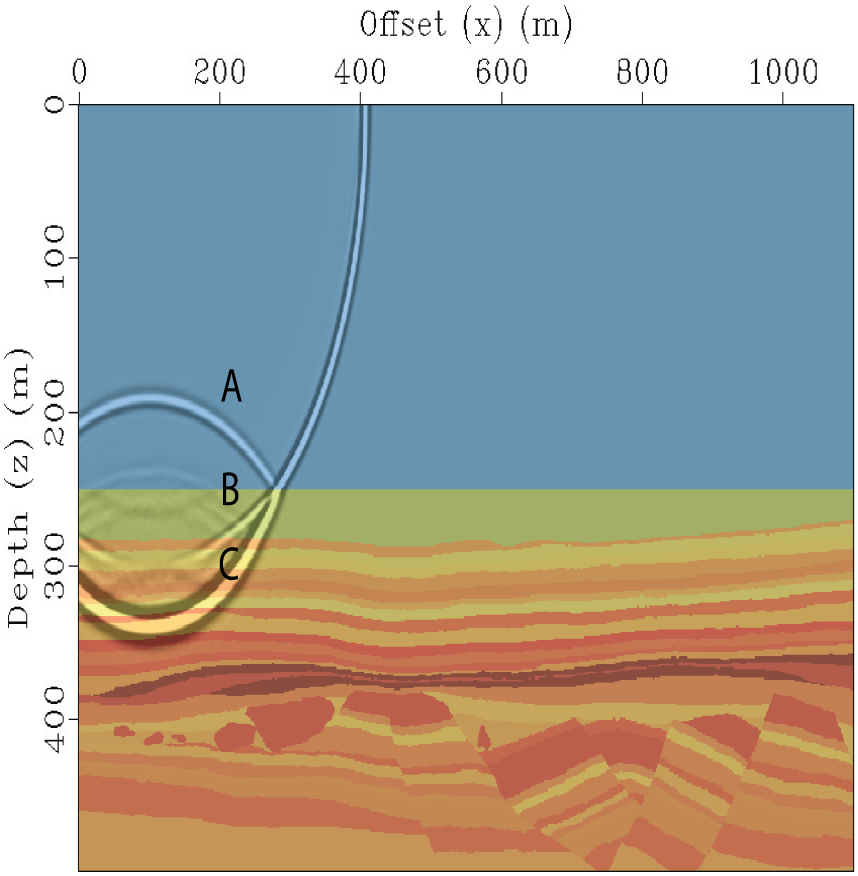

Figure 6.11: Time snap of the wavefield for shot #130 at time 0.23 seconds overlain by the P-wave velocity model for local model #130.

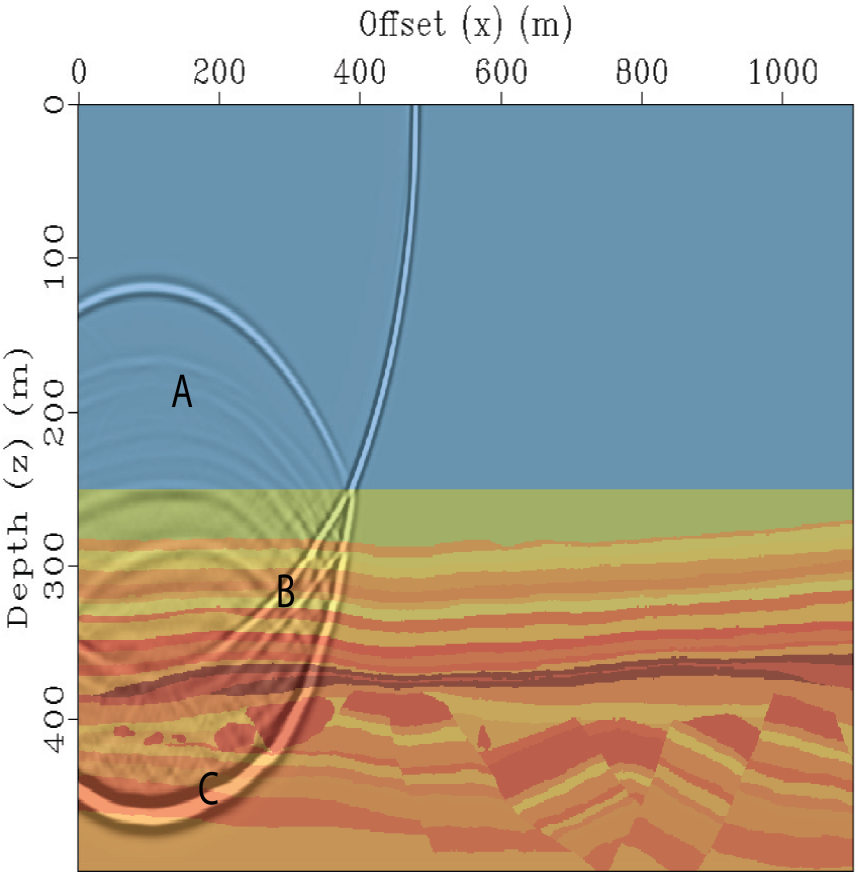

Figure 6.12: Time snap of the wavefield for shot #130 at time 0.28 seconds overlain by the P-wave velocity model for local model #130.

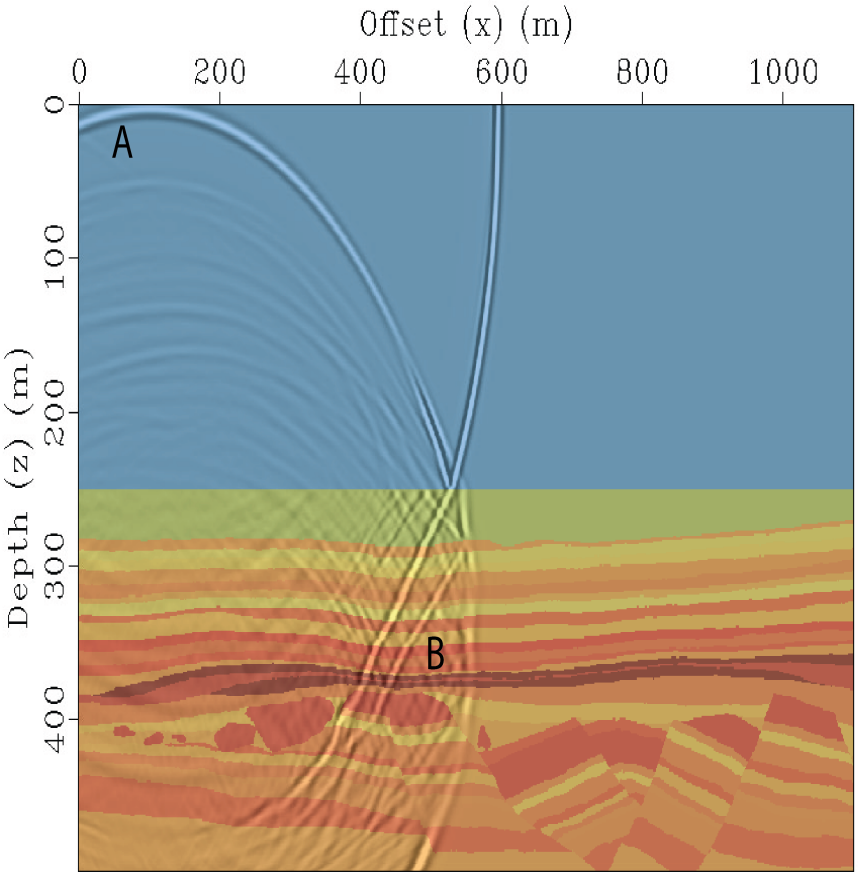

Figure 6.13: Time snap of the wavefield for shot #130 at time 0.36 seconds overlain by the P-wave velocity model for local model #130.

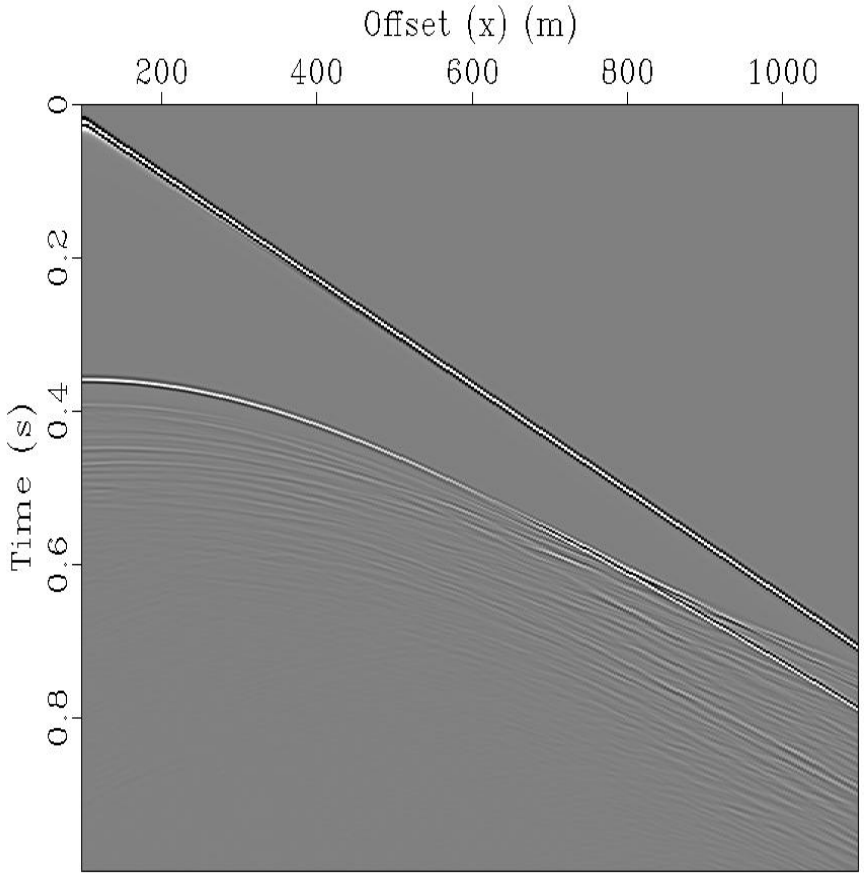

Figure 6.14: Data recorded at the receivers for shot #130. Notice the time delay of the source signal by the arrival of the head wave slightly below zero time.

6.3 Seismic data processing and imaging

The goal of this section is to present the processing flow and imaging techniques used to create the final results and images in this thesis. Numerous test with differing processing parameters and sequences were run and in the end the processing flow introduced in Table 6.3 was found to give the best

Processing Flow
Read data
Resample data
Source correction
Set geomtery
Mute direct wave
Bandpass frequency filtering with 20-250 Hz
Sort data to common midpoint
Import real velocity model and convert from depth to time
Convert interval velocities to rms velocities
Correct normal moveout
Stack NMO data
Pre-stack Kirchhoff time migration

Table 6.3: The processing flow used in thesis.

results. Detailed parameters for each processing sequence will not be presented in this thesis but a short description of and motivation for is given. Seismic processing is often a time consuming process and due to the time constraint of this thesis a limited number of processing flows and algorithms were tested.

The first processing steps were to edit the data and ready it for further processing. Correction of the time delay in the source signal to put the wavelet at zero phase was the first step and it is observed by comparing Figure 6.14 with Figure 6.15. Figure 6.16 display the shot gather for shot #130 after the direct wave was removed. All geometry settings were reset after the acquisition so that the data origin was put at shot #1 and the time axis was resampled to 0.01 seconds to minimize the computation time. A bandpass filter between 20Hz and 250Hz was applied to the data to remove low and high frequency noise from the data.

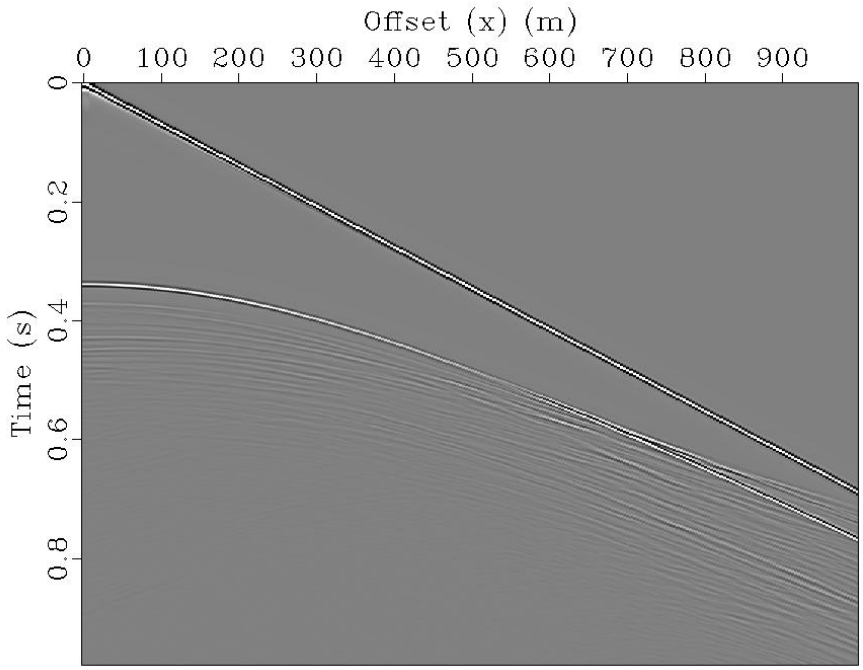

Figure 6.15: Shot #130 with the time delay in the source signal corrected.

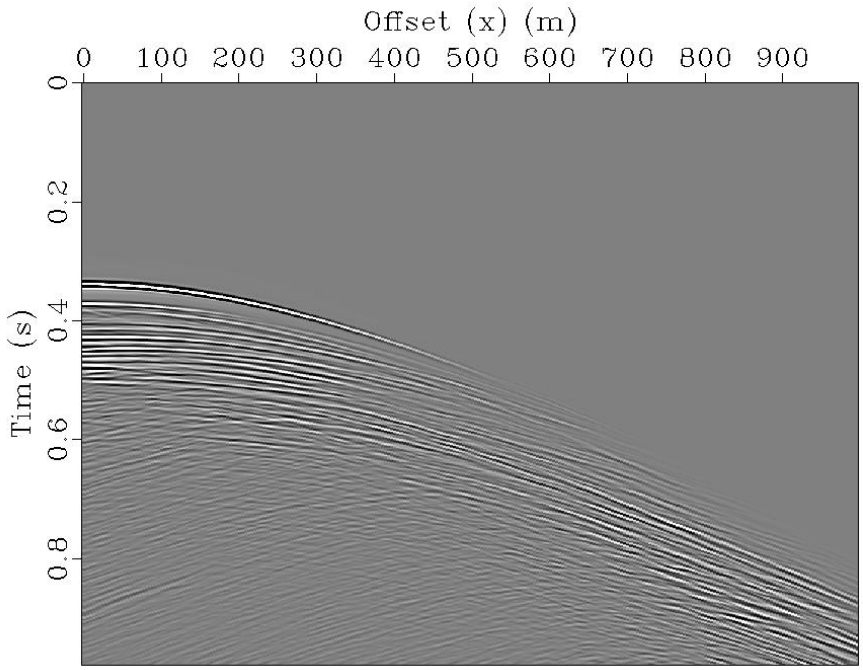

Figure 6.16: Shot #130 with the source signal corrected and the head wave muted. Notice how the reflectors in the lower part of the data are stonger.

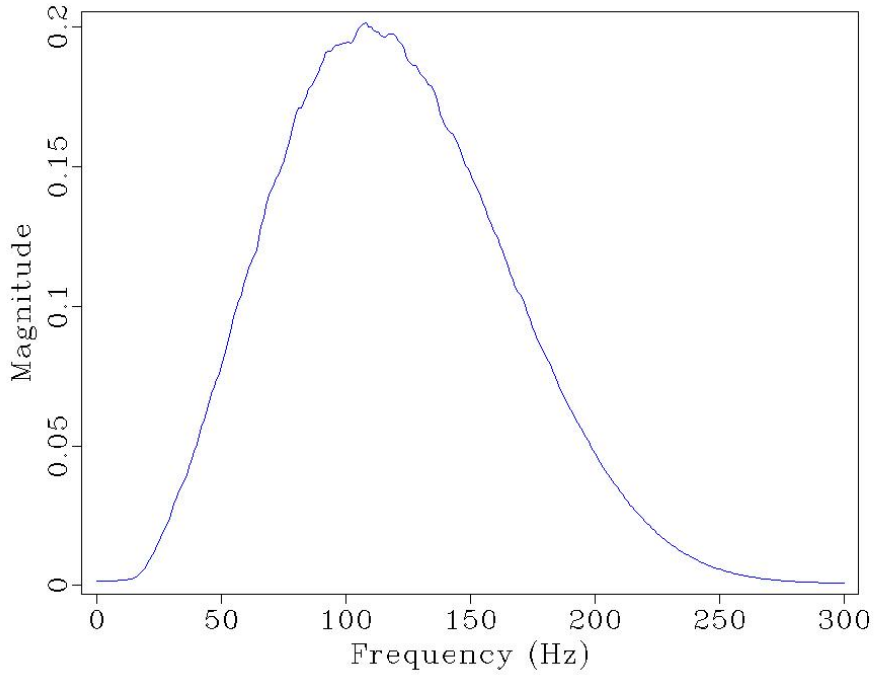

Figure 6.17: Frequency spectrum of shot #130 with band pass filter applied.

Real velocities were imported in the processing to obtain the best possible result and the velocity model in Figure 6.4 was used in this thesis. The interval velocity model was first expanded along the time axis by attaching a copy of the model where all velocities are doubled at the bottom the model as seen in Figure 6.18. This was done to deal with some software issues that arose when the model was strechted from time to depth which is observed at the bottom of Figure 6.19 where Figure 6.18 is stretched to time. Figure 6.20 shows the velocity model used this thesis; it was obtained by transforming the interval velocities in Figure 6.19 into RMS velocities using Dix equation. The depth of the model is 500 m and if one assumes an average velocity of $2000\frac{m}{s}$ the reflections from the lowest part of the model should arrive at 0.5

seconds. The RMS velocity model in Figure 6.20 is cut at 0.6 seconds in this figure as all data below is assumed to be numerical noise.

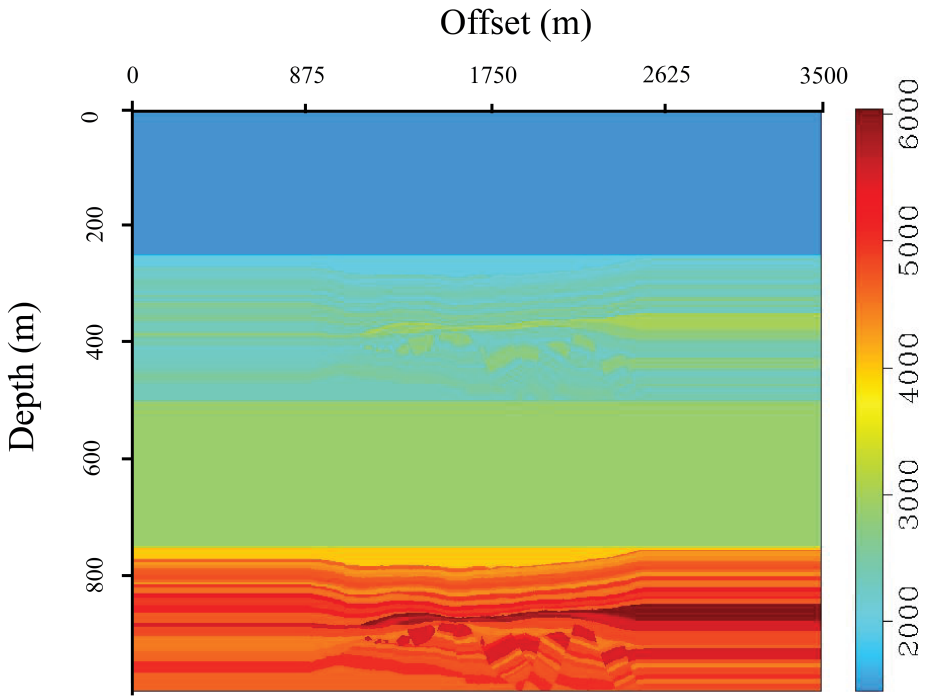

Figure 6.18: Interval velocity model in depth where a copy of the model where all velocities are multiplied with 2 is placed at the bottom of the velocity model seen in Figure 6.7. The values range from 1500 to over 6000 m/s

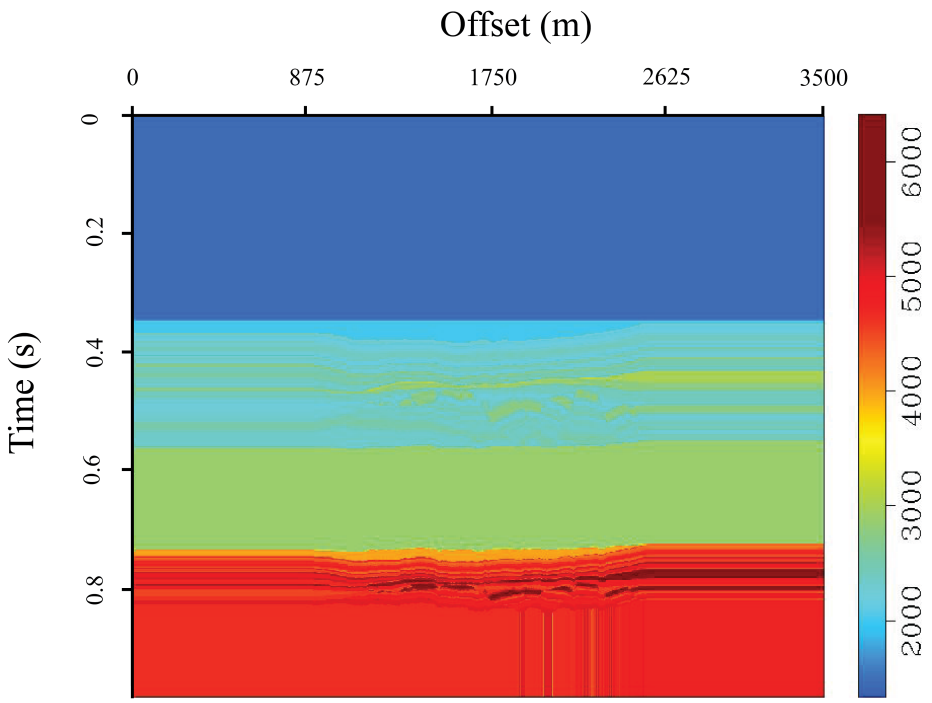

Figure 6.19: Interval velocity model in time. Note the vertical lines at the bottom of the model which caused problems in the processing flow before the extra model was attached on the time axis.

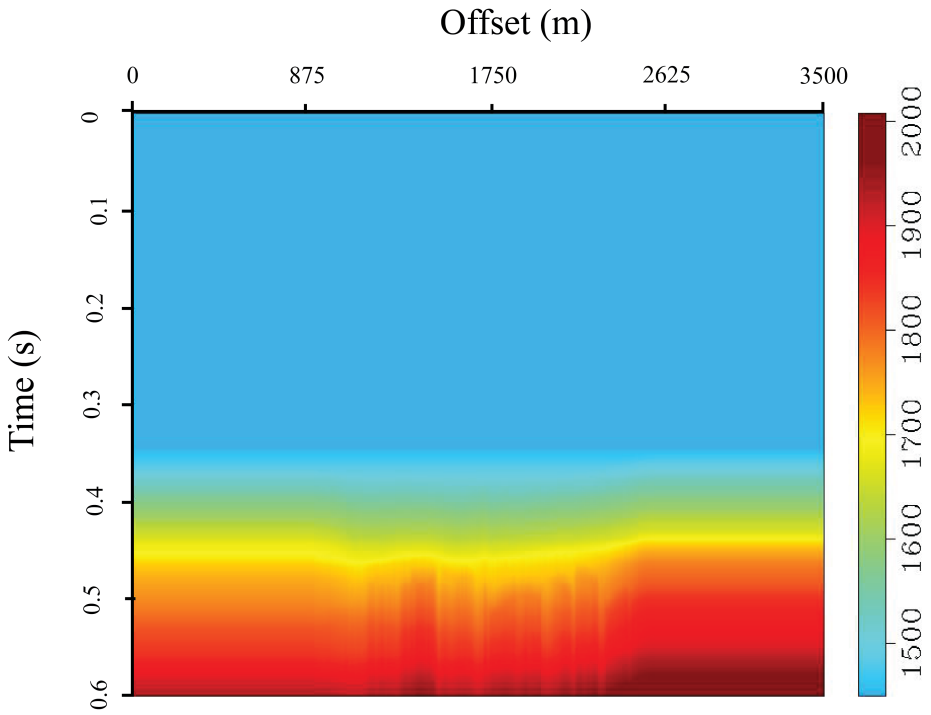

Figure 6.20: RMS velocity model constructed from Figure 6.19. In this figure the model is cut 0.6 seconds as all data below are assumed to be numerical noise.

The data was sorted to common midpoint data as seen in Figure 6.21 and a NMO correction was carried out and the result can be seen in Figure 6.22. The correction seems to have flattened the data well although at large offsets and signals arriving after 0.5 seconds the nmo correction appears to be less effective. For data below 0.5 seconds the poor result was attributed to the fact that most of this data was assumed to be noise. The NMO corrected data was stacked and Figure 6.23 display the stack from the midpoint at 1000 m to 2500 m with the time axis cut at 0.6 seconds. The stacked section can be divided into two different parts with an upper clean section containing

several relatively flat reflectors and a lower chaotic section. No gain was applied to this data would account for some of the more dimmed reflectors in the lower section. Several diffractions was identified in both in the upper and lower part but the majority is found in the lower section.

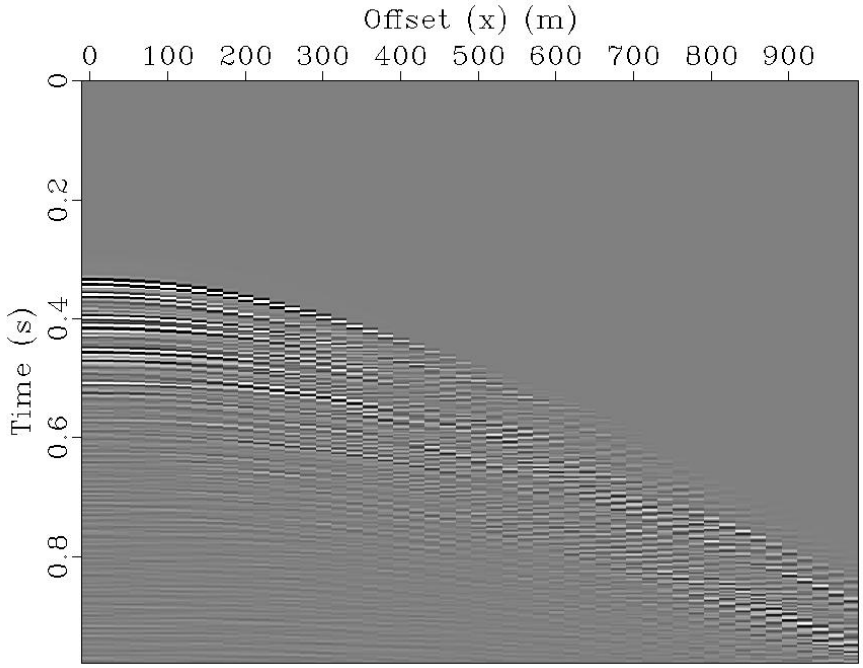

Figure 6.21: Common midpoint gather for midpoint #750 near the the center of the model

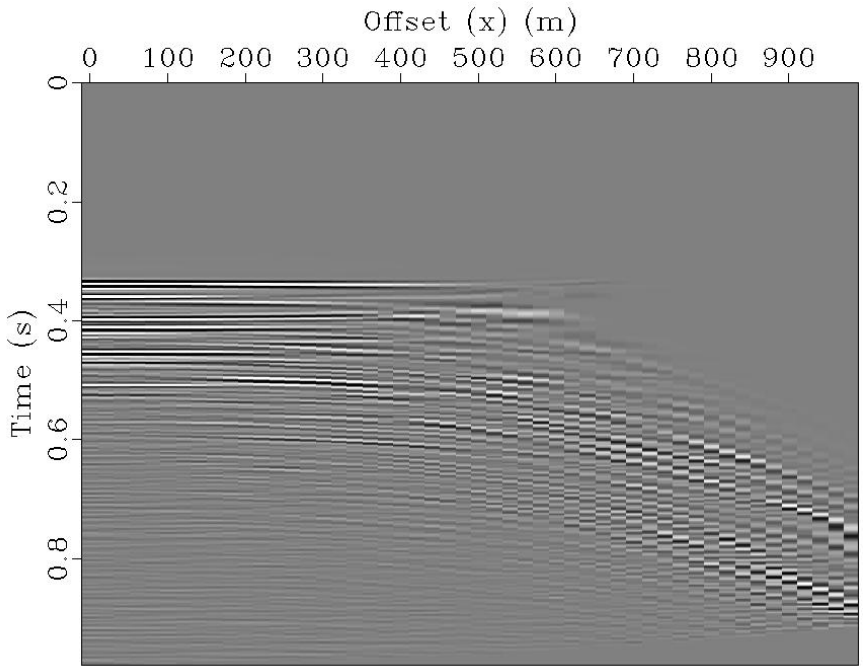

Figure 6.22: NMO corrected cmp #750 near the the center of the model. For large offsets

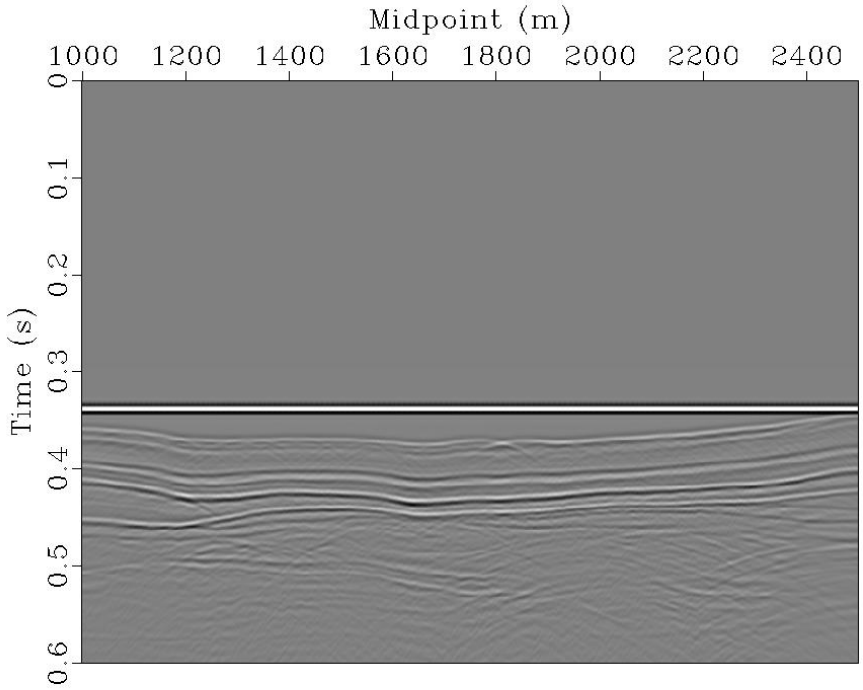

Figure 6.23: Stacked data of the modeled area between midpoint #1000 and #2500 where the time axis is cut at 0.6 seconds.

The final processing step was to migrate the data so that energy is moved to the correct reflection point. Pre-stack time migration was used to migrate the data in this thesis and the resulting image is seen in Figure 6.24 and Figure 6.25 where the window has been cut to the area covered by the Kvalvågen model. A power gain with t^3 was used in both images.

A comparison between migrated data in Figure 6.25 with the unmigrated stacked data in Figure 6.23 display a marked improvement in data quality. The gained migrated data contain stronger amplitudes especially in the lower part of the section when compared to the stacked section. The diffractions observed in the stacked section have disappeared in the migrated image and

the lower chaotic section is much more coherent in the migrated section. Several reflectors are observed in the lower part of the section and also the faults in the central and right hand side of the model are identified in the lower part of the migrated image. Reflections from all the small fault related slide blocks are observed on the left hand side of the section.

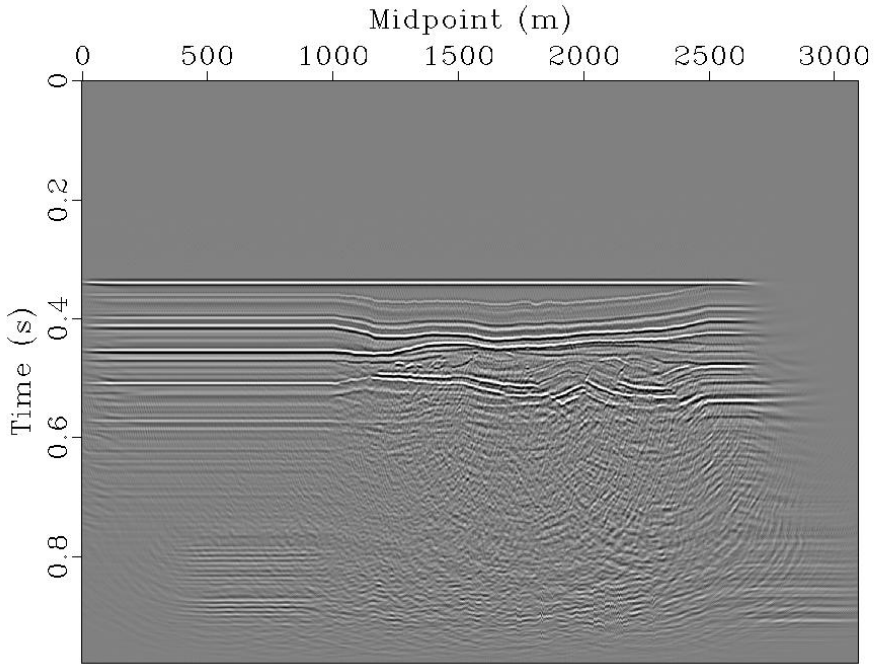

Figure 6.24: Final image processed with a 2-D Prestack Kirchhoff time migration. A power gain with 3 to the power of time (t) was applied after migration.

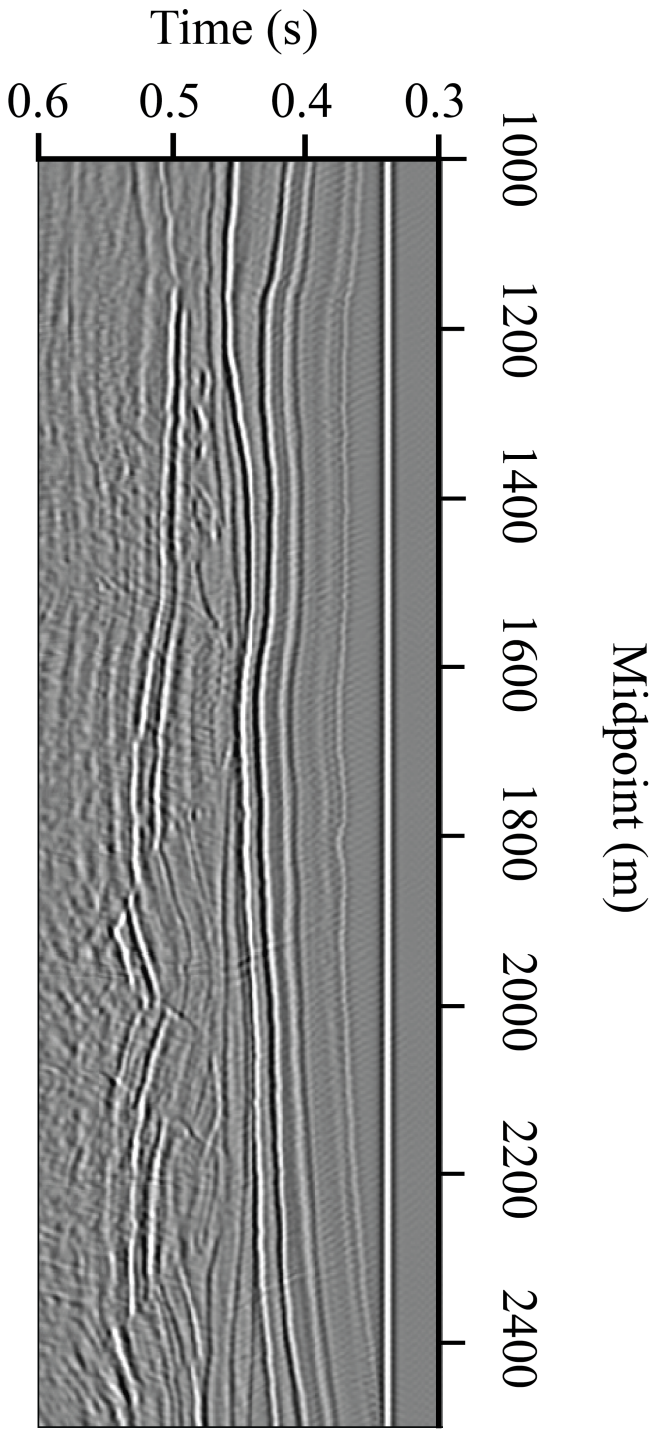

Figure 6.25: Seismic image of the section converted by the Kvalvågen

6.4 Altering the acquisition parameters

Acquisition set up and parameters used to produce the results in the section above are pretty ideal when compared to the parameters used in conventional seismic acquisitions. Shot and receiver spacing are typical around 25 m and 12.5 m respectively in a conventional survey and the frequencies are usually in a range of 5-100 Hz although shallower sections as the one studied here contains more high frequency content. In an attempt to simulate more realistic acquisitions two new datasets were acquired, one with the ricker wavelet centered at 50Hz instead of 100Hz and one with a shot spacing of 20 m and receiver spacing of 10 m.

Figure 6.27 contains the section shot with a 50Hz source signal and the frequency spectrum of shot #130 in the data is seen in Figure 6.26. The section was found to contain the same noise in the upper part as found in Figure 6.25. The lower part of the section is more distorted and it is harder to recognize the reflectors. The complex fault blocks are not as easy to identify as in the section with 100Hz source, smaller faults especially. One of the small slide blocks on the left hand side of the section is not recognized The reflectors are thicker which is to be expected from lower frequencies.

The seismic image in Figure 6.28 was produced was acquired with a wider shot and receiver spacing and the image contains noticeably more noise and poorer data quality than the seismic section in Figure 6.25. The data looks less continuous and broken up in the direction of the offset axis. The layers and faults in the lower part of the section are still visible and the thickness of the reflectors is equal to that of the seismic in Figure 6.25.

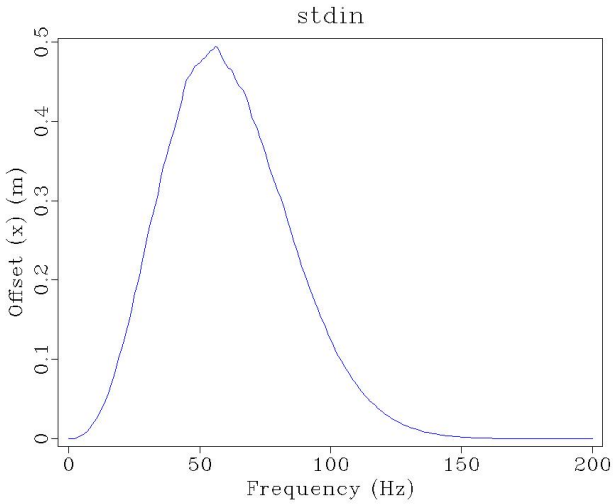

Figure 6.26: Frequency spectrum from shot #130 of the collected with a 50Hz ricker wavelet seen in Figure 6.27

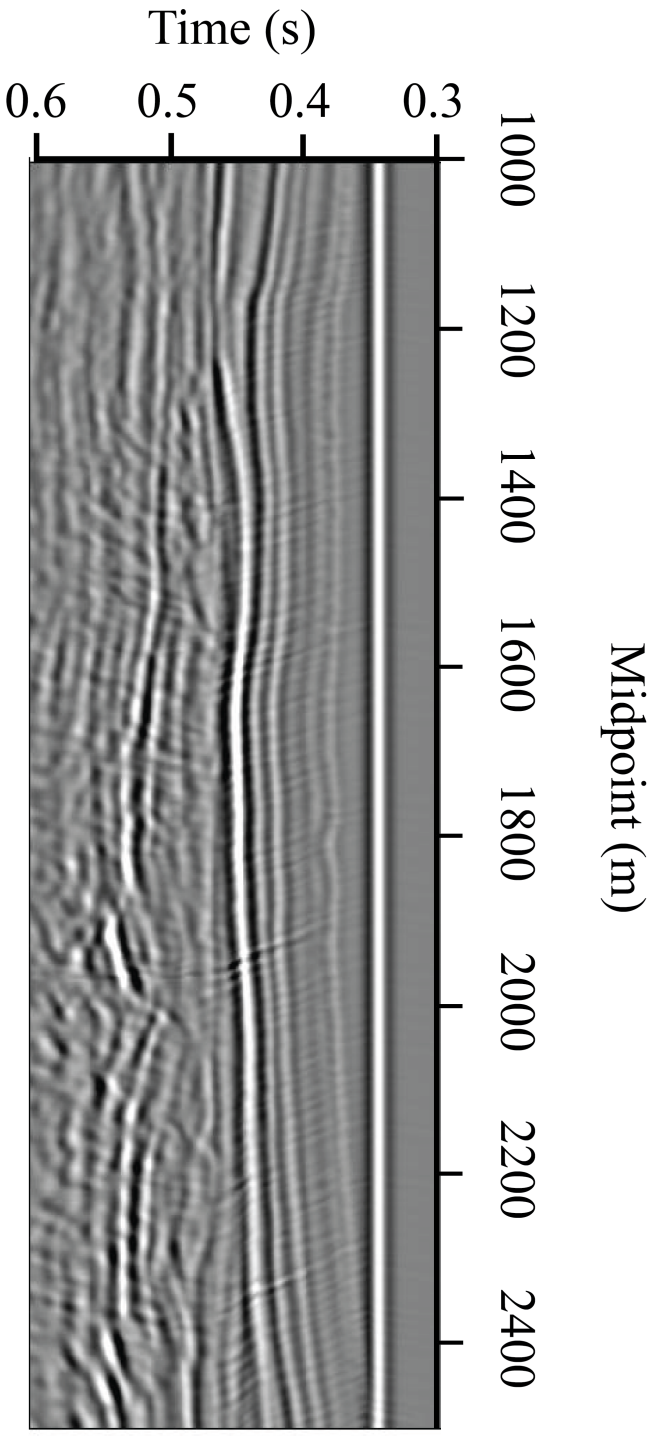

Figure 6.27: Migrated image of data acquired with a 50Hz impulse where all other acquisition parameters are the same as in Figure 6.25

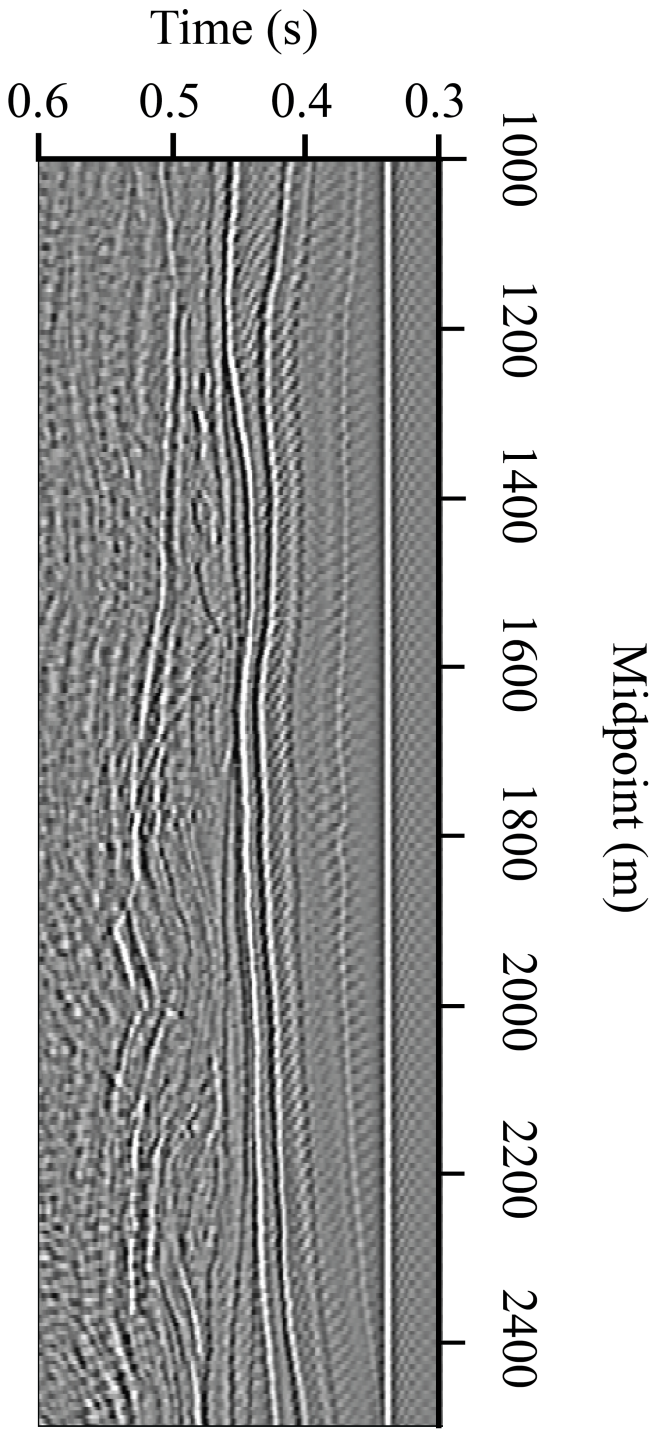

Figure 6.28: Migrated image of data acquired with 10 m receiver spacing and 20 m shot spacing to simulate a more realistic acquisition scenario.

6.5 Reverse time migration

Depth migration was tested to find the best possible result from the modelling. A reverse time migration was tested using the correct velocity models was run to produce a the best possible final result. Figure 6.29 show the final migrated image in depth, several marked improvements over the previous Kirchhoff migrated time sections are found. The fault blocks in the lower part of the section are imaged better as is the reflectors below the fault blocks.

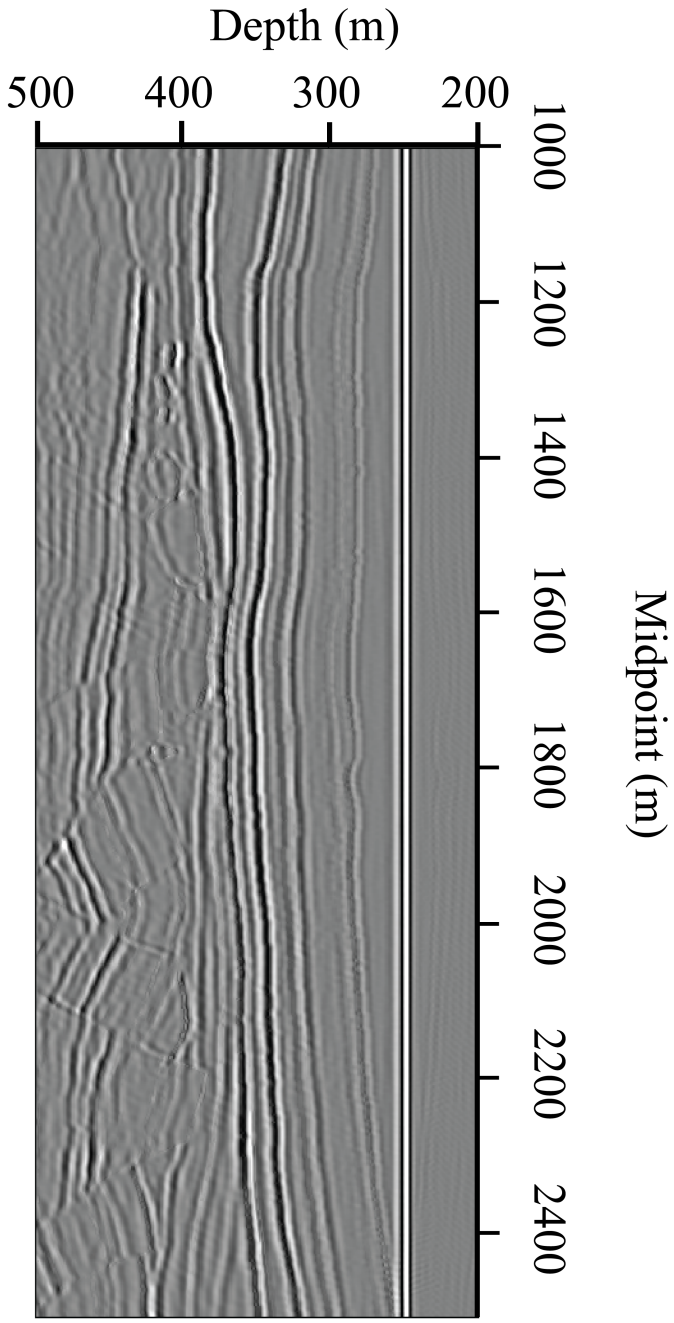

Figure 6.29: The imaged section produced with a reverse time migration. Note that the image is in depth and not time.

Chapter 7

Discussion

The goal of this chapter is to discuss the results of the geological and seismic modelling in the thesis. Explanations of some of the observed effects and seismic features in the final seismic images are given. Issues and sources of error in the experiments are discussed and examples of how the errors affects the final results are given.

Building a geological and petrophysical model of the Kvalvågen outcrop in Petrel designed for forward seismic modeling in Madagascar was one of the primary results of this thesis. The model is detailed and made of 1x1x1 meter grid cells which is sufficient to model small scale geological variations. However inner bed variations and small scale facies changes are not included in the model and the earth model is still not as complex or varied as the actual earth. Nor does the homogeneous nature of the model take anisotropy, cracks or fractures into account. Constant values are used for velocities and density within each layer and accounts for another simplification when comparing with how the earth actually is. These simplifications in the earth model give

a less continuous model and the results is that layer transitions are more marked in the model and thereby easier to image.

The purpose of this study was to examine how detailed seismic sections actually are and what sort of geological details are lost due to limited seismic resolution. Figure 6.29 show the best results in this thesis and most of the layers in the geological model are found in the section. The faults in the section are also imaged really well and it is observed that they are present throughout the section. The slide blocks in the section are also identified on the final section and both a top and bottom reflector is identified for the two biggest ones whereas only single reflections are identified for the three smaller blocks. They are detectable but not resolvable on the seismic section. These results were produced in an experiment where the velocities and densities used in the migration were the correct ones taken from the petrophsical models, the source signal contains a lot of high frequencies, the shot and receiver spacing in the acquisition where much closer than in a real survey and there was no acquisition noise although some numerical noise was present. Considering this it is still an impressive results as is shows how much information is contained in the seismic signal if it is extracted perfectly and demonstrates how well an geological section can be imaged by seismic.

Figure 6.25 gives one a better idea of how a real seismic section shot over a geological section like the one found at Kvalvågen would look like. Pre-stack time migration is still the most widely used migration technique in the oil and gas industry and although the RMS velocities are taken from the input model, the results still reflects an actual seismic section better than Figure 6.29. The discrepancies between the time and depth migrated

sections are especially seen around the faults where the time migrated section has problems imaging the deeper parts of the faults and the layers beneath them. Figure 7.1 show time migrated section with a the P-wave velocity model stretched from depth to time on top to demonstrate which layers in the model are imaged. As expected are the strongest reflectors located where there are marked changes in velocity are found.

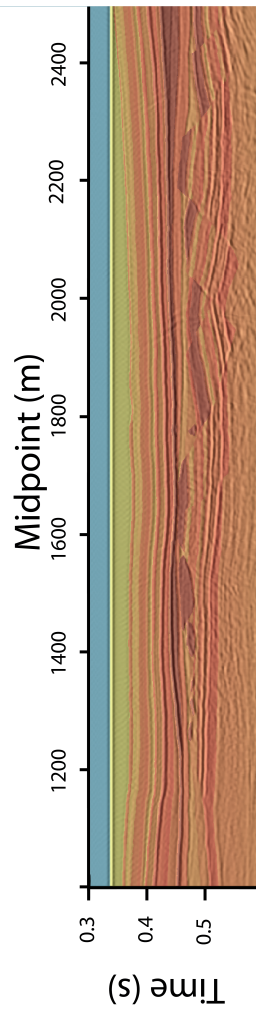

Figure 7.1: Image of the Pre-stack time migrated section with the P-wave velocity model put on top to illustrate which layers are imaged and the correlation between model and migrated image. The velocity model was here stretched from depth to time.

Comparisons of the results from the 100 Hz ricker wavelet source in Figure 6.25 and the 50 Hz ricker wavelet in Figure 6.27 illustrate how much information is lost by excluding the frequencies from 150-250 Hz from the frequency spectra. The upper part of the section with the more horizontal layers appear relatively similar but discrepancies are found in the lower parts

and especially are the faults imaged better with higher resolution. Reflectors appear less sharp in the 50 Hz section and somewhat smeared together. Two strong reflectors in the lower part of the faulted section in Figure 6.25 are are not resolved as two separate reflectors in the 50 Hz section illustrate the difference in vertical resolution between the two sections. Using an acquisition geometry more similar to those used in the oil and gas (Figure 6.28) industry had no effect on the vertical resolution of the image but the spatial resolution was effected. Especially dispersion phenomena in the horizontal layers of the upper section increase when shot and receiver spacing are increased.

Figure 7.2 illustrate the effect frequency content has on seismic resolution. Filtering out the high frequencies (Figure 7.2 (a)) give a more blurred image with thicker reflectors while retaining only the high frequencies as seen in Figure 7.2 (c) gives a much clearer image resembling the depth migrated section. Filtering out frequencies will also remove important information from the seismic signal but in a structural complex cases as the one studied here it can improve fault interpretation.

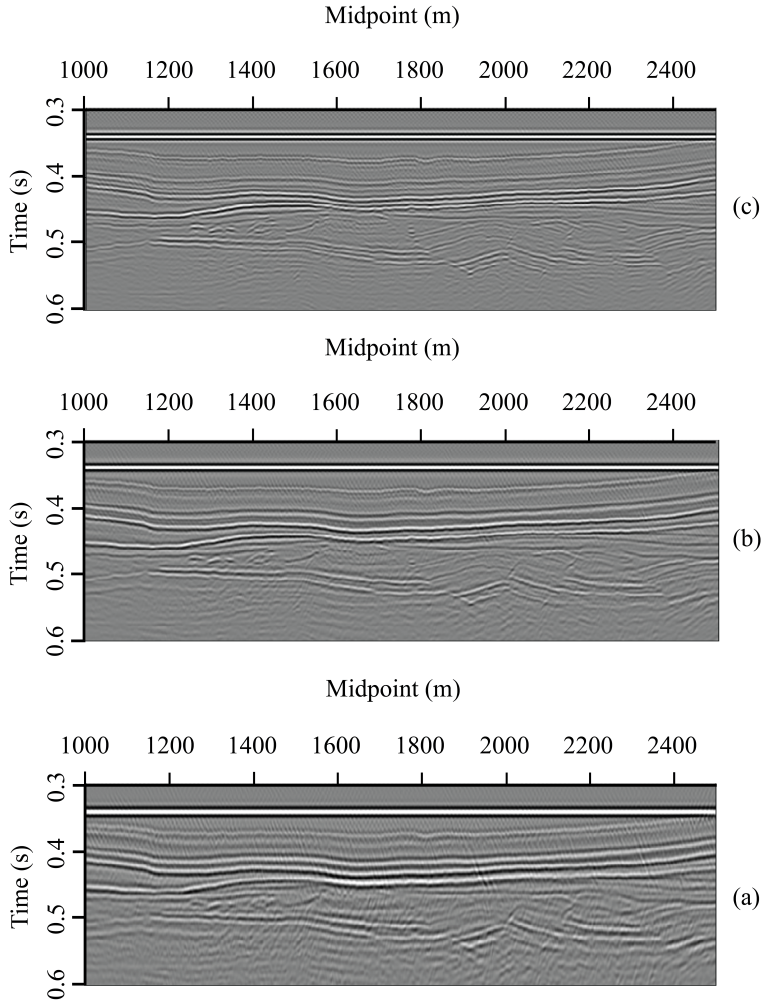

Figure 7.2: Pre-stack time migrated section (Figure 6.25) with various frequency filters applied. (a) Frequnecies between 20-100 Hz filtered, (b) frequencies between 50-250 Hz filtered, (c) frequencies between 100-250 Hz filtered.

Vertical seismic resolution is defined in Chapter 11 of Yilmaz (2001) as a quarter of the dominant wavelength $\lambda = \frac{v}{f}$ where v is the velocity and f is the dominant frequency. For the low velocity layers near the seabottom the resolution should be

$$\frac{\frac{1}{100Hz} * 2000\frac{m}{s}}{4} = 5meters$$

and for the highest velocity layers in the model should be

$$\frac{\frac{1}{100Hz} * 3000\frac{m}{s}}{4} = 7.5meters$$

The smallest of the slide blocks in the geological model is 5 meters in depth but it is still resolved with a top and bottom in the Figure 6.29 which indicates that the vertical resolution is even better than the theoretical one in this ideally migrated dataset.

One of the observed errors in the experiments were the noisy patterns of almost vertical lines that appeared especially in the upper parts of the time migrated section. It is also found to a lesser degree in the depth migrated section where it also distorts the upper part of the section and makes the reflectors there less continuous than the ones further down in the section. The phenomena appear more marked in the Pre-stack time migrated sections and this is thought to be a result of the migration process. These phenomena were attributed to dispersion in the upper layers. Holberg (1987) defined that "For FD modelling of realistic seismic phenomena, a spatial sampling rate of more than 20 points per shortest wavelength is needed". For the upper parts of the model the frequencies are up to 250 Hz and the shortest wavelength 8 m which results in dispersion as the grid points are located with a meters spacing and the grid is to large to avoid dispersion effects. In order to avoid dispersion the shortest wavelength should atleast be 20 meters.

The Ricker wavelet used in the modelling are also a source of error as it relatively homogeneous compared to a real seismic pulse and the frequency spectra is narrower and more focused around the peak frequency than what one would expect a real seismic pulse to be. The ricker wavelet also produce

two fairly prominent side lobes that influence the final image and makes it harder to interpret and separate thin layers.

Originally this thesis was meant to be done in 3D and the geological model was made in 3D, but time constraints lead to the decision of doing the seismic modelling part in 2D. The modelling algorithm is such that adding n layer of cells in the third dimension will increase the computation time with n^2, which means that expanding the grid one meter in the third dimension will increase the computation time with a factor of four. With a 2D setup and 120 processors running the computation time of the seismic modelling were around 1.5 hours in this thesis and in order to simulate the effect of 3D wave propagation an extra 10-20 cells had to be included in the model which would increase the computation time of the seismic modelling to 150-600 hours.

The Kvalvågen model can be used in several ways for further research projects. 3D seismic modelling can be acquired with the proper time and by decreasing the sampling intervals of both space and time. Full waveform inversion can be tested on this model by creating initial models for velocities and density and the results from reverse time migration indicate that the model is well suited for such experiments. Simulating time-lapse seismic can be performed by simply changing some of the parameters in the model to simulate a change fluid content or pressure. Modelling of CSEM data is also possible if a new resistivity property model can be produced and the results could be compared with the results from the seismic modelling to study how CSEM and seismic data correlate. The acquisition geometry could be altered and one could study how the faults are imaged from the different azimuths than parallel to fault strike direction.

Chapter 8

Conclusion

A method for creating geological and petrophysical models in the Petrel software based on a image of a geological outcop was found. The models were then converted to the RSF format used by the Madagascar software package in order to simulate a seismic acquisition and the resulting data were processed to create images of the section.

Investigating a single shot and comparing the wave field with actual model gave insights as to how which layers in the subsurface where imaged and it was found that the thin layers gave reflections in this thesis. This method also proved useful to identify wave phenomena and illustrate the effects of varying rock parameters have on wave propagation.

Reverse time migration as expected proved superior to the pre-stack time migration in imaging the section and this is attributed to the fact that interval velocities are used in the reverse time migration and RMS veloctites are used in the Kirchhoff pre-stack time migration. A geological anomaly of only 5 meters is resolved on the final section and all faults in the model are

imaged. The depth migrated section manages to image the entire faults and the reflectors beneath the faults which the time migrated sections fail to image completely.

High frequency content in the ricker wavelet used as a source explain the high resolution images created and shortening the frequency spectra of the source result in a final image that is more blurred and distorted with thicker reflectors and the faults are also imaged poorly. However all of the slide blocks are observed on the lower frequency section even though they are not resolved with both a top and bottom reflector. Using an acquisition set-up with larger spacing between shots and receiver has a small to no impact on vertical resolution but enhances the dispersion effects of the image. Filtering out frequencies from the final image was found to be helpful tool in resolving and interpreting faults and complex structures.

The final images in this thesis are excellent seismic sections especially when one considers that the section is only 250 meters deep below the sea bottom. Explanations for the high quality of the final images include perfect migration velocities, absence of multiples, high frequency content in the source signal, homogeneous layers in the earth model and constant value parameters in the geological layers which results in a less smooth geological model.

Bibliography

Alaei, B. (2005). "Seismic forward modeling of two fault-related folds from the Dezful Embayment of the Iranian Zagros mountains". In: *Journal of Seismic Exploration*.

Armour, A. et al. (2003). *THE MILLENNIUM ATLAS: PETROLEUM GEOLOGY of the CENTRAL and NORTHERN NORTH SEA*.

Arntsen, Børge (2013). *Reservoir Seismics - Lecture Notes*.

Ayzenberg, M. (2008). "Three-dimensional seismic diffraction modeling". phd. NTNU.

Carcione, J. (2002). "Seismic Modeling". In: *Geophysics* 64, pp. 1304–1325.

Castagna, J.P., M.L. Batzle, and R.L. Eastwood (1985). "Relationship between compressional-wave and shear-wave velocities in clastic silicate rocks". In: *Geophysics*.

Gjelberg, J. and R. J. Steel (1995). "Helvetiafjellet formation (Barremian-Aptian), Spitsbergen: characteristics of a transgressive succession". In: *Sequence Stratigraphy on the Northwest European Margin Proceedings of the Norwegian Petroleum Society Conference*. Ed. by R.J. Steel et al. Vol. 5. Norwegian Petroleum Society Special Publications. Elsevier, pp. 571–593. DOI: 10.1016/S0928-8937(06)80087-1.

Graves, R. W. (1996). "Simulating seismic wave propagation in 3D elastic media using staggered-grid finite differences". In: *Bulletin of the Seismological Society of America*.

Hilterman, . J. (1970). "Three-Dimensional seismic modeling". In: *Geophysics* 35.6, pp. 1020–1037. DOI: 10.1190/1.1440140.

Holberg, O. (1987). "Computational Aspetcs of the choice of operator and sampling interval for numerical differentiation in large-scale simulation of wave phenomena". In: *Geophysical Prospecting*.

Ikelle, L. T. and L. Amundsen (2005). *Introduction to Petroleum Seismology*. Tulsa, OK: Society of Exploration Geophysics. ISBN: 9781560801702. DOI: DOI:10.1190/1.9781560801702.

Johansen, S. E., E. Granberg, et al. (2007). "Decoupling of seismic reflectors and stratigraphic timelines: A modeling study of Tertiary strata from Svalbard". In: *Geophysics* 72.5, pp. 273–280.

Johansen, S. E., S. Kibsgaard, et al. (1994). "Seismic modeling of a strongly emergent thrust front, West Spitsbergen fold belt, Svalbard". In: *AAPG Bulletin*.

Krebes, E. S. (Apr. 2004). "Seismic Forward Modeling". In: *CSEG RECORDER*, pp. 28–39.

Kristensen, T. B. and M. Huuse (2012). "Multistage erosion and infill of buried Pleistocene tunnel valleys and associated seismic velocity effects". In: *Geological Society, London, Special Publications*.

Levander, A. R. (1988). "Fourth-order finite-difference P-SV seismograms". In: *Geophysics* 53.11, pp. 1425–1436.

Midtkandal, I. and J. P. Nystuen (2009). "Depositionalarchitecture of a low-gradient ramp shelf in an epicontinental sea: the lower Cretaceous of Svalbard". In: *Basin Research*.

Midtkandal, I., J. P. Nystuen, et al. (2008). "Lower Cretaceous lithostratigraphy across a regional subaerial unconformity in Spitsbergen: the Rurikfjellet and Helvetiafjellet formations". In: *Norwegian Journal of Geology*.

Mørk, A. et al. (1999). "Mesozoic lithostratigraphy". In: *Lithostratigraphic Lexicon of Svalbard, Review and Recommendations for Nomenclature Use. Upper Palaeozoic to Quaternary Bedrock*. Ed. by W.K.Dallmann. Norsk Polarinstitutt, Tromsø, pp. 127–214.

Nemec, W. et al. (1988a). "Anatomy of collapsed and re-established delta front in Lower Cretaceous of eastern Spitsbergen; gravitational sliding and sedimentation processes". In: *AAPG Bulletin*.

— (1988b). "Exhumed rotational slides and scar infill features in a Cretaceous delta front, eastern Spitsbergen". In: *Polar Research*.

Onderdonk, N. and I. Midtkandal (2010). "Mechanisms of collapse of the cretaceous helvetiafjellet formation at Kvalvågen, eastern Spitsberge". In: *Marine and Petroleum Geology* 27.10, pp. 2118–2140. ISSN: 0264-8172. DOI: 10.1016/j.marpetgeo.2010.09.004.

Praeg, D. (2003). "Seismic imaging of mid-Pleistocene tunnel-valleys in the North Sea Basin - high resolution from low frequencies". In: *Journal of Applied Geophysics* 53.4, pp. 273–298. ISSN: 0926-9851. DOI: 10.1016/j.jappgeo.2003.08.001.

Steinsbø, K. G. (2012). "Forward Seismic Modelling - Work Flow and Case Study From the North Sea". Project. NTNU.

Tøndel, R. (1997). "A seismic modelling study of Mediumfjellet, Spitsbergen - with emphasis on finite difference modelling". Masters. NTNU.

Worsley, D. and O. J. Aga (1986). *The geological history of Svalbard- Evolution of an arctic archipelago*. Stavanger: Den Norske Stats Oljeselskap a.s.

Yilmaz, O. (2001). *Seismic Data Analysis*. Tulsa, OK: Society of Exploration Geophysicists. ISBN: 9781560801580. DOI: DOI:10.1190/1.9781560801580.

List of Figures

List of Tables

Appendix A

SConstruct scripts

This appendix contains the SConstruct scripts used in thesis study for both forward seismic modeling and seismic processing.

A.1 Single Shot

Shot number 130

```
### Python command
from rsf.proj import *

#=============================================================
# SConstruct for single shot seismic modeling
#=============================================================

### Resampling
Flow('rho','Rho','window d3=60')
```

```
Flow('vp','Vp','window d3=60')
Flow('vs','Vs','window d3=60')

### Plotting input models
Result('rho','window min1=150 | grey color=j title="Density model of shot
#130" scalebar=y bias=1750')
Result('vp','window min1=150 | grey color=j title="Vp model of shot #130"
scalebar=y bias=2250')
Result('vs','window min1=150 | grey color=j title="Vs model of shot #130"
scalebar=y bias=750')

### Cutting model to fit shot #130
Flow('rho-shot130','rho','window min2=200 max2=1300 | put o2=0')
Flow('vp-shot130','vp','window min2=200 max2=1300 | put o2=0')
Flow('vs-shot130','vs','window min2=200 max2=1300 | put o2=0')

### Plotting shot model models
Result('rho-shot130','window min1=150 | grey color=j title="Density model
of shot #130" scalebar=y bias=1750')
Result('vp-shot130','window min1=150 | grey color=j title="Vp model of
shot #130" scalebar=y bias=2250')
Result('vs-shot130','window min1=150 | grey color=j title="Vs model of shot
#130" scalebar=y bias=750')

###Modeling
Flow('spike',None,'spike n1=10000 d1=0.0001 k1=200 mag=1000')
```

```
Flow('ricker','spike','ricker1 frequency=100')
Flow(['rec','szz','sxx','sxz','vz','vx'],['rho-shot130','vp-shot130','vs-shot130','ricker'],"'
fd2dewe
verb=1
free_surface=0
rho=$SOURCES[0]
vp=$SOURCES[1]
vs=$SOURCES[2]
source=$SOURCES[3]
rec=$TARGETS[0]
szz=$TARGETS[1]
sxz=$TARGETS[3]
sxx=$TARGETS[2]
vz=$TARGETS[4]
xx=$TARGETS[5]
xsource=100
zsource=3
sampsnaps=5
zrec=6
xstart=100
xend=1100
xinc=4
"')

End()
```

```
Result('ricker','window n1=500 | graph title="Ricker"')
Result('rec','grey color=g title="Receivers"')
Result('szz','grey transp=y poly=y yreverse=y title="Wavefield"')
Result('sxz','grey color=j title="Wavefield"')
```

A.2 Acquisition

Acquisition of 100Hz data. Gathered with parallell modeling

```
#### Importing libraries
from rsf.proj import *
from rsf.recipes import msimmod

#=============================================================
# SConstruct for seismic acquisition
#=============================================================

### Setup model

Flow('rho1','Rho','window d3=60')
Flow('vp1','Vp','window d3=60')
Flow('vs1','Vs','window d3=60')

Flow('rho2','rho1','span axis=2 n=1100 place=1')
```

```
Flow('vp2','vp1','span axis=2 n=1100 place=1')
Flow('vs2','vs1','span axis=2 n=1100 place=1')

Flow('rho','rho2','span axis=2 n=1100 place=2')
Flow('vp','vp2','span axis=2 n=1100 place=2')
Flow('vs','vs2','span axis=2 n=1100 place=2')

Result('Rho','grey bias=2300 scalebar=y title="Density Model"')
Result('Vp','grey bias=2000 scalebar=y color=j title="P-wave Velocity Model"')
Result('Vs','grey bias=1000 scalebar=y color=j title="S-wave Velocity Model"')

#### Modeling

# Parameter setup
par = {
'dim':2,
'nshots':260,
'dt':0.0001,
'nt':10000,
'surface':0,
'local_models':1,
'ghost_border':20,
'shotgeometry':'shots.rsf',
'workingpath':'/work/knutgus/6mrec/kval3'
}
par['receiver'] = {'xstart':100,'xinc':4,'xend':1100,'z':6}
```

```
par['size']={'nx':1100}
par['inc']={'x':10}
par['start']={'x':0}
par['end']={'x':2600}
par['source']={'x':100,'z':3}

msimmod.param(par)

# Wavelet
msimmod.wavelet('source',100,1000,200,par)
Result('source','graph title="Source wavelet"')

# Modeling
msimmod.split('rho','vp','vs',par)
msimmod.mod('source','rho','vp','vs',par)
msimmod.cat('data',par)

End ()
```

A.3 Processing

Processing of 100Hz data

```
from rsf.proj import *
```

```
#=============================================================
# SConstruct for processing flow
#=============================================================

#— Resampling
Flow("shots1","data","window j1=10 f1=200")
Flow("shots3","shots1"," put o1=0 o2=0 o3=0")

#— QC plot of shot
Flow("shot2","shots3","sfwindow min3=1500 max3=1500")
Result("shot2", "sfgrey")

#— Mute
Flow("shots2-mute", "shots2", "sfmutter half=n v0=1450 t0=0.1 tp=0.4")

#— Spectrum of shot
Flow("shot2-spectrum","shots3","sfwindow min3=1500 max3=1500 | sfspec-
tra all=y")
Result("shot2-spectrum", "sfgraph")

#— Bandpass Filter
Flow("shots2","shots3","sfbandpass flo=20 fhi=250")

#— QC plot of muted shot
Flow("shot2-mute","shots2-mute","sfwindow min3=1500 max3=1500")
```

```
Result("shot2-mute", "sfgrey")

#— Sort to cdp
Flow("cmps2", "shots2-mute", "shot2cmp mask=msk.rsf half=n")

#— QC of CMP's
Flow("cmp2","cmps2","window min3=1500 max3=2000")
Result("cmp2", "sfgrey")

Flow("vint2", "vint", "window f2=201 n2=3098")
Flow("vint1", "vint2", "window j2=2")
Result("vint1","grey color=j scalebar=y min=1400 bias=2200")
#— Convert depth velocity model to time
Flow("vins", "vint1","depth2time dt=0.001 nt=980 velocity=vint1.rsf")
#— Convert stacking velocities
Flow("vels1", "vins", "vint2vrms")
Flow("vels", "vels1", "put o2=0")
Result("vels","grey min=14000 bias=1500 scalebar=y color=j")

#— Nmo
Flow("nmos2", "cmps2", "sfnmo half=n velocity=vels.rsf str=0.15")

#— QC plot of nmo corrected cmp
Flow("nmo2","nmos2","window min3=1200 max3=1800")
Result("nmo2", "sfgrey")
```

```
#— Stack
Flow("stack2", "nmos2", "sfstack | sfwindow max1=0.6 min2=1000 max2=2500")
Result("stack2", "sfgrey")

#— Migration
Flow("tcmp","cmps2","transp plane=23 memsize=1")
Flow("migstack", "tcmp", "sfmig2 vel=vels.rsf half=n")
Flow("migstack-final","migstack","window min1=0.3 max1=0.6 min2=1000
max2=2500")
Result("migstack", "sfgrey")
Result("migstack-final", "sfgrey")

#— Post processing
Flow("mig","migstack-final","sftpow tpow=3")

End()
```

A.4 RTM

```
##### Importing libraries
from rsf.proj import *
from rsf.recipes import msimmod

#To get localpath correct
```

```
import os
env = Environment (ENV = {'PBS_JOBID': os.environ['PBS_JOBID']})


##### Creating models
Flow('rho','Rho','window d3=60 | span axis=2 n=1100 place=1 | span axis=2
n=1100 place=2')
Flow('vp','Vp','window d3=60 | span axis=2 n=1100 place=1 | span axis=2
n=1100 place=2')
Flow('vs','Vs','window d3=60 | span axis=2 n=1100 place=1 | span axis=2
n=1100 place=2')


#### Muting direct wave


Flow('mute','data','sfmutter half=n v0=1450 t0=0.1 tp=0.4')


##### Splitting into single files
for i in range(260):
count=100+(10*i)
Flow('Flow('

##### Modeling
# Parameters
par = { 'dim':2,
'nshots':260,
'dt':0.0001,
```

```
'nt':10000,
'surface':0,
'ghost_border':20,
'local_models':1,
'workingpath':'/work/knutgus/6mrec/kval3/RTM',
'localpath':'/scratch/pbstmp.' + env['ENV']['PBS_JOBID'] +'/',
'modbuffer':500
}
# Setup local models
# Source and receivers
par['source'] = 'z':3,'x':100
par['receiver'] = 'z':3,'xstart':100,'xinc':4,'xend':1100
par['size'] = 'nx':1100
par['inc'] = 'x':10
par['start'] = 'x':0
par['end'] = 'x':2600
msimmod.param(par)


# Splitting models
msimmod.split('rho','vp','vs',par)


# Migration
msimmod.mig('source','rho','vp','vs',par)


# Stacking image
```

targets = ['Flow('image',targets,'stackoffset')

End()

Appendix B

Petrel Appendix

This appendix contains data from Petrel and work flows from Petrel which was cut from the final draft of the thesis.

B.1 Model builing in Petrel

This sections contains a more in depth guide as to how the geological and petrophysical models were made in Petrel.

B.1.1 Importing and localizing outcrop

The method for building models in this study was to import an image of the model into Petrel and interpret horizons and surfaces from this picture which will serve as the basis for the model. In this study natural tracing paper was used to create the preliminary model by placing it on top of a picture of the outcrop and sketching a lithological model.

The first step step in this process was to import the picture of the preliminary model into Petrel and locate it in the world in order to be able to track the horizons. This done by using the locate in world function under the settings tab of the picture in Petrel as seen in Figure B.1. By checking the independent edges button it is possible to determine the spatial position of the pictures edges and thereby determine the geometry required for the model.

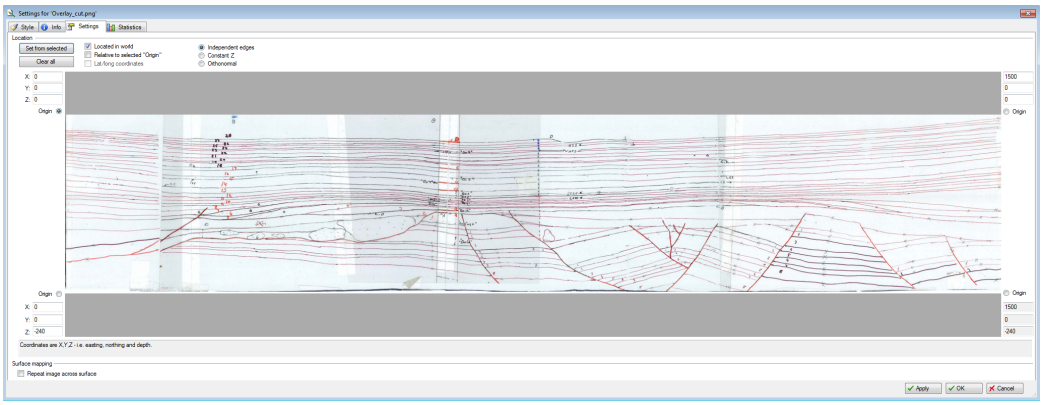

Figure B.1: The settings tab of imported picture in Petrel which shows how a picture can be located in the world using the independent edges button. Each corner of the image has an x,y and z coordinate which is set to fit the desired geomtery.

Creating surfaces

Digitizing the interpreted geological layers in the imported image was done to create surfaces in Petrel, surfaces that will be the framework of the geological model. The process create/edit polygons was used in this study to track the horizons on the imported image, in Figure B.2 it can be observed how points are traced on top of the model in the imported image.

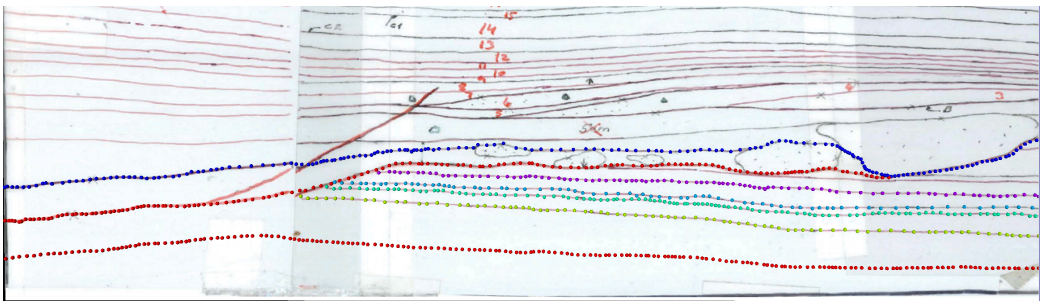

Figure B.2: Image snipped from Petrel which shows how the create/edit points process has been used to interpret/digitize horizons on the imported image. Note that "younger" horizons cut older so as to stay on top.

Creating surfaces in Petrel is a fairly simple task acomplished thorugh the Make/Edit surface process. This process takes some input data and interpolates them to create a surface, surface size, grid size and interpolation method are determined as part of the process. Figure B.3a displays the dialog box for creating surfaces. Input data, grid size and geometry are set in this box. Under the algorithm tab the interpolation algorithm is determined and in this study the "closest" algorithm is used. It adheres to the data points in the input only, and as a result, the surfaces it produces are just extended along the axis perpendicular to the data points as seen in Figure B.3b.

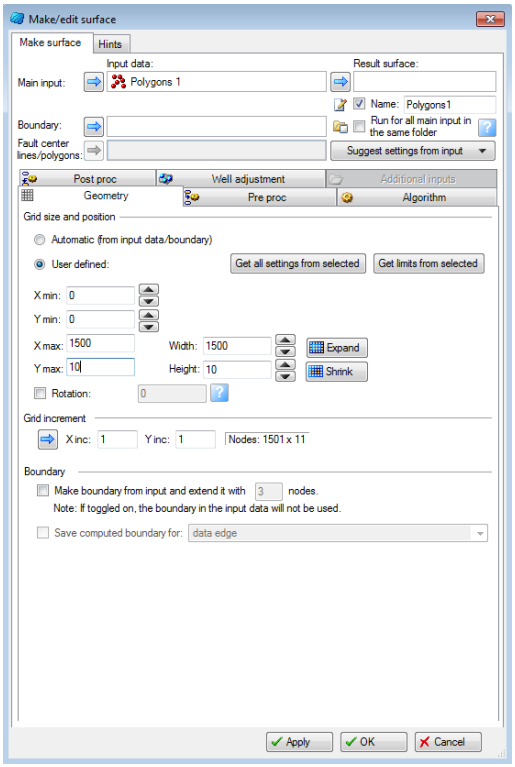

(a) Image of the Make/edit points process from Petrel. The input data, which in this study were points, is chosen here as is the geometry of the surface

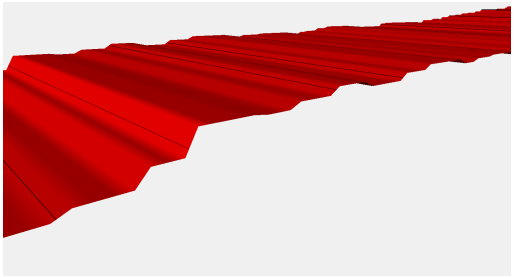

(b) Image of a surface taken in Petrel, the surface is really only expanded out perpendicular to the input points according to the geometry set in the Make/edit surface process

Figure B.3

B.1.2 Create grid

After a surface was created for all the horizons in the imported image creating a model grid was the task at hand. Regular grids can be created quite easily in Petrel using two flat surfaces, the Make simple grid process and layering process. Two constant depth surfaces that will serve as the top and bottom of the model has to be made first and this is quickly done in the Make/edit surface process by choosing the Artificial algorithms and constant z value

under the Algorithm tab. Now these two surfaces will serve as the input in the Make simle grid process; it is also important to rember to use an approriate grid size. Dividing the model into cells is done in the layering process by setting the number of vertical cells in the model as seen in Figure B.4b.

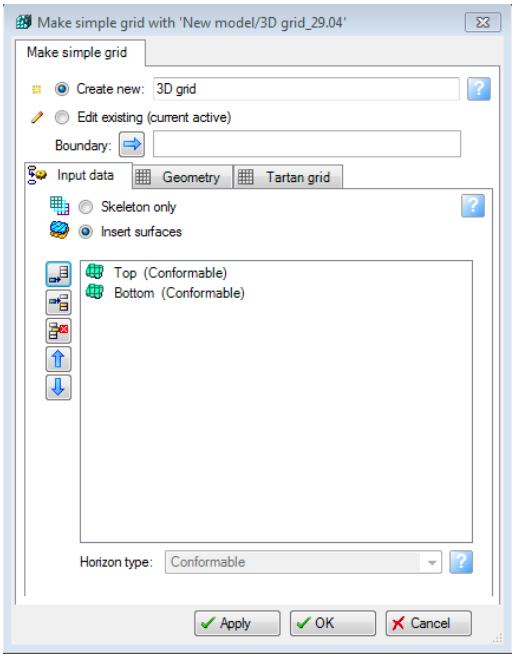

(a) Picture showing the Make/edit points process from Petrel with a top and bottom surface imported as input data. The input data, which in this study were points, is chosen here as is the geometry of the surface

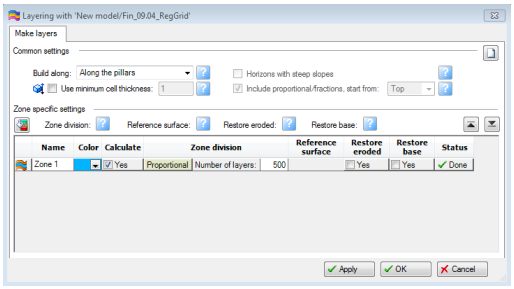

(b) Image of the layering process in Petrel used to make vertical cells in a Petrel grid

Figure B.4

B.1.3 Petrophiscal models

Populating the grid with rock properties was done through the Geometrical modeling process in Petrel and accomplished by using the Assigne between surfaces and polygons method. Figure B.5a shows how the previously created

surfaces was used as input and all cells inbetween them were given a constant value. To speed up the process and make it easier to update the various models, a facies model was created by giving a specific value to each layer in the model. Then the built in calculator in Petrel was used to assign the desired property value for each layer in the facies model as seen in Figure B.5b

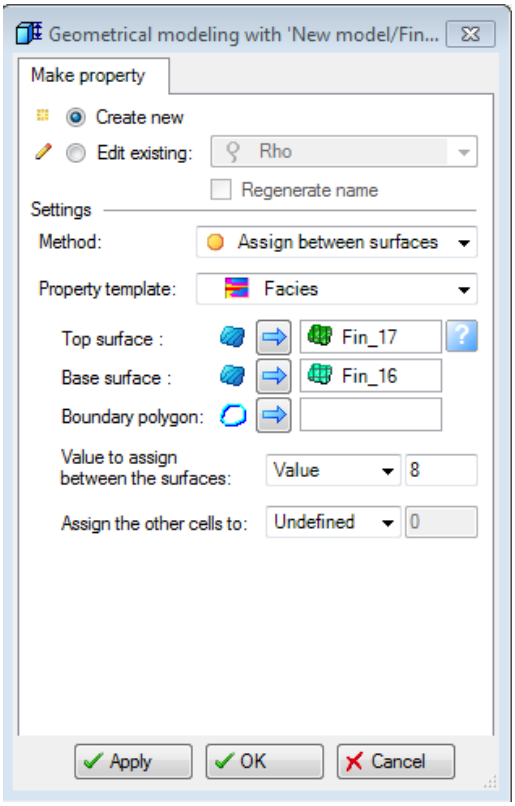

(a) The Geometrical modeling process in Petrel with the Assign between surfaces and polygons method chosen

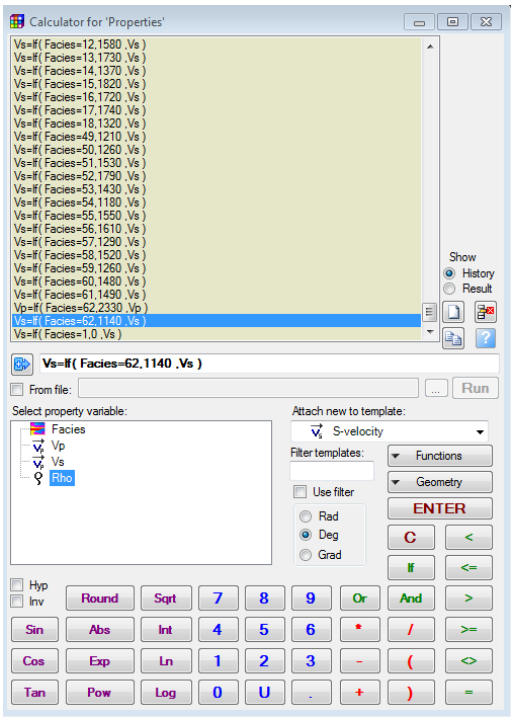

(b) The calculator with an example of how the

Figure B.5

One problem that arose in this study was that in some places two or more surfaces was supposed to be lying on top of each other but small spaces existed between them. This was due to some difficulties in placing the individual

points on top of each other when digitizing the horizons on the imported picture and proved a problem as in some places a couple of cells of a underlying layer would pop up in the "younger" layer above. This was solved by tracking the underlying horizon above the top one. Then after having converted them to surfaces go into the calculations tab in the settings of the underlying surface and use the Z>=A button with the overlying surface as the reference A and place the surface underlying surface at the exact same place as the top one, this is demonstarted in Figure B.7.

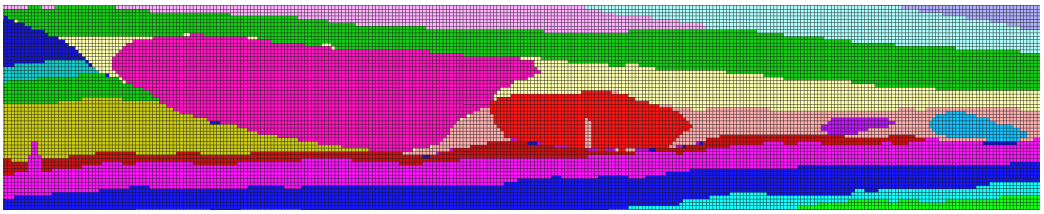

Figure B.6: Picture taken from Petrel of the facies model demonstrating the issue with cells from underlying layers appearing in overlying layers

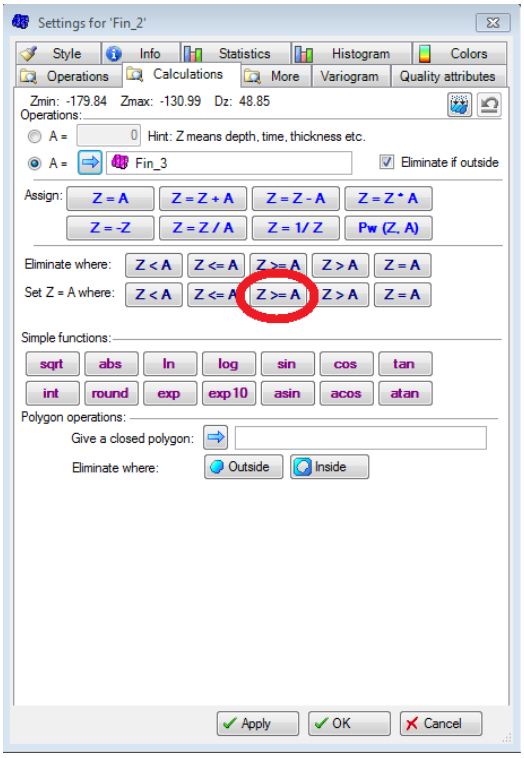

Figure B.7: The calculations tab in the settings of surfaces was used to force the surface to never have a greater value than a reference surface A by choosing the Z>=A option as circeled in red. This was done top put several surfaces directly on top of each other in areas such as faults where several surfaces was overlapping.

After all kinks were worked out the end results looked a lot better as can be seen by comparing Figure B.6 with Figure B.8 where the changes are applied. Figure B.9 shows the finished facies model in a 3D window.

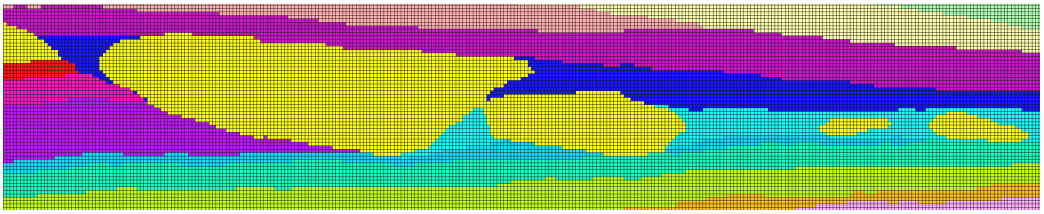

Figure B.8: Image from Petrel with same model as in Figure B.6 but after the fix shown in Figure B.7 has been applied. All the overlapping cells are now gone. The difference in colors between this figure and Figure B.6 come from slightly different color scales and the fact that some minor changes have been done to model

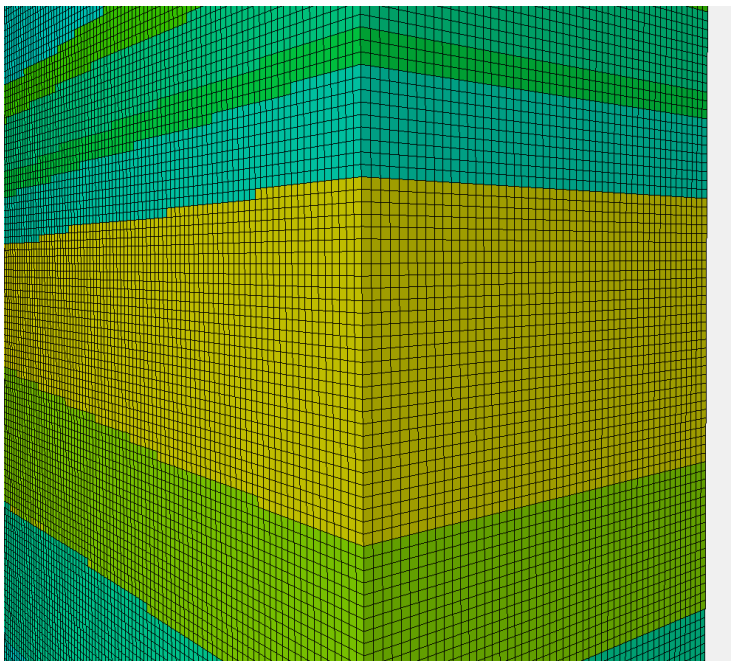

Figure B.9: Picture taken from Petrel displayings parts a finished model in a 3D window

B.2 Tabel and Models

The tabel of all the velocities and densities used in this thesis is found in Table B.1 while the property models as seen in petrel are found in Figure B.10, Figure B.11 and Figure B.12.

Table B.1: Velocities and densitites of the geological model. The layers are stacked vertically with layer 1 being the water layer, layer 2 being the seabottom and so forth.

Layer number	Density $[\frac{kg}{m^3}]$	Vp $[\frac{m}{s}]$	Vs $[\frac{m}{s}]$
1	1.00	1500.00	1000.00
2	2.13	2000.00	1200.00
3	2.23	2340.00	1550.00
4	2.45	2150.00	1250.00
5	2.48	2200.00	1190.00
6	2.31	2350.00	1310.00
7	2.34	2400.00	1400.00
8	2.49	2300.00	1240.00
9	2.43	2180.00	1330.00
10	2.28	2480.00	1290.00
11	2.43	2280.00	1270.00
12	2.54	2650.00	1620.00
13	2.37	2460.00	1580.00
14	2.34	2580.00	1730.00
15	2.51	2350.00	1370.00
16	2.49	3020.00	1820.00
17	2.51	2770.00	1720.00
18	2.42	2920.00	1740.00
19	2.55	2420.00	1320.00
20	2.52	2260.00	1210.00
21	2.43	2320.00	1260.00
22	2.35	2550.00	1530.00
23	2.32	2750.00	1790.00
24	2.45	2390.00	1430.00
25	2.53	2230.00	1180.00
26	2.42	2410.00	1550.00
27	2.29	2520.00	1610.00
28	2.44	2290.00	1290.00
29	2.31	2430.00	1520.00
30	2.43	2370.00	1260.00
31	2.36	2380.00	1480.00
32	2.40	2510.00	1490.00
32	2.52	2330.00	1140.00

Figure B.10: P-wave wave model from Petrel

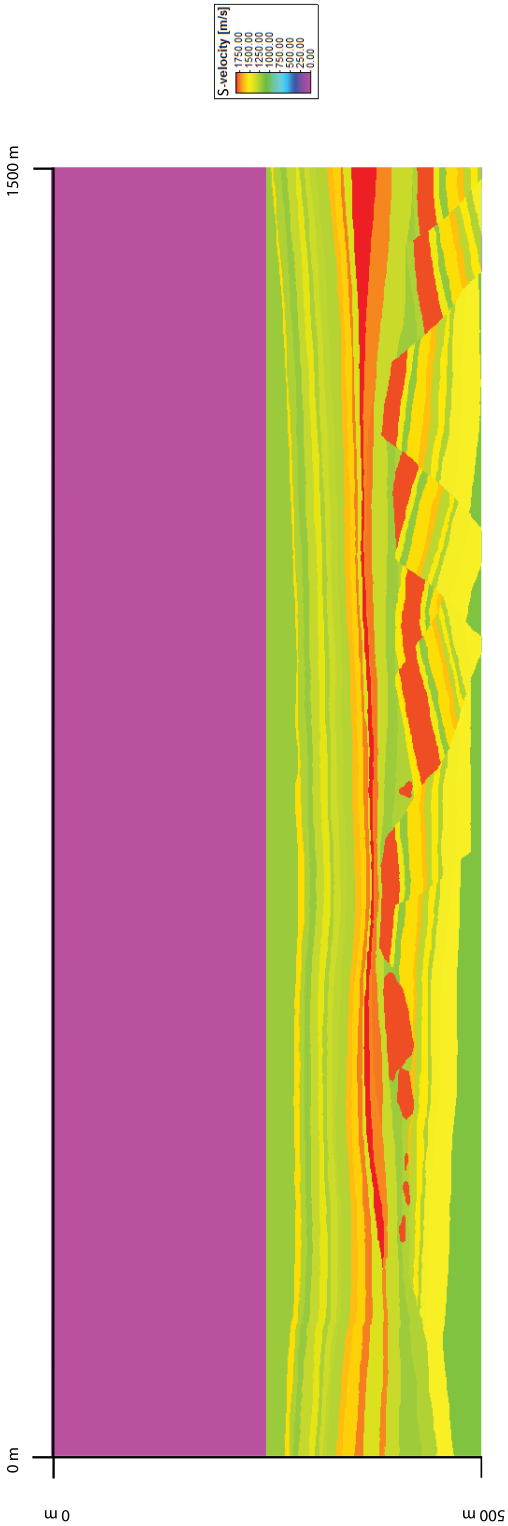

Figure B.11: Shear wave velocity model from Petrel

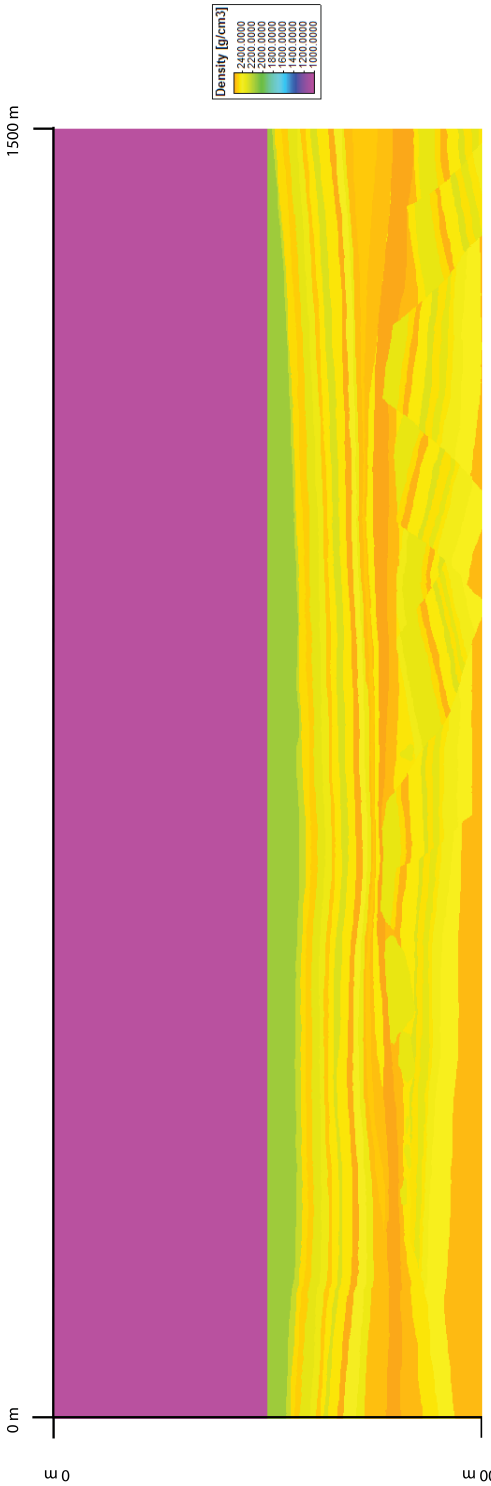

Figure B.12: Density model from Petrel

Appendix C

Madagascar

This chapter will include data, examples and work flows from Madagascar which were not included in the main body of the thesis. Data from both modelling and processing will be presented here.

C.1 Seismic Modelling

In this study forward seismic modeling is performed to acquire synthetic seismic data and the Madagascar software package is used to present simulate seismic surveys. This section presents the seismic modeling method and work flow used in this study and demonstrate how Madagascar is used to produce the results found in this thesis. A short presentation will be given about each step of the process aswell as some of the more important Madagascar programs that is used in the thesis.

C.1.1 Importing and editing Models

The first step in the process was to import the models from Petrel into Madagascar which basically involves converting them from the Eclipse format used in Petrel to the RSF format that is used in the Madagascar package. The package sfpetread was written by Børge Arntzen for this purpose and all it requires is the files resulting from the export Eclipse grid with properties function in Petrel and that they be in the same folder on the system you are working on, Figure C.1 shows the Vp model after it has been converted into the RSF format.

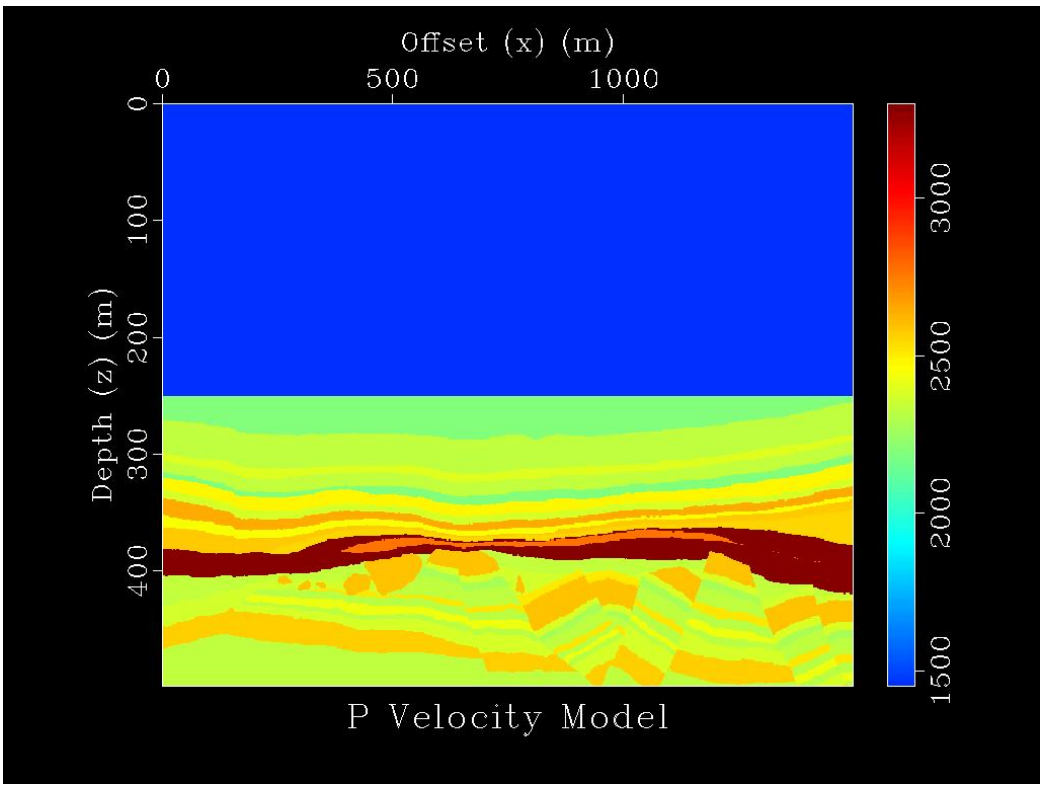

Figure C.1: The P velocity model after it has been converted to the RSF format for use in the Madagascar package

An attractive feature with Madagascar is that it can be used to do some simple editing on the models after they have been imported which are simple processes in Madagascar but would be very time consuming to do in Petrel. Perhaps the most important one in this study was the program sfspan that was used to add padding at the ends of the model, a process which would have been much more time consuming in Petrel and could also have caused some performance issues in Petrel when working on a much larger model. Figure C.2 shows the model from Figure C.1 after sfspan has been used to add 6km of padding to the model. The program sfwindow can also be useful if it's necessary to resample the model to a coarser grid size so as to decrease

computation time.

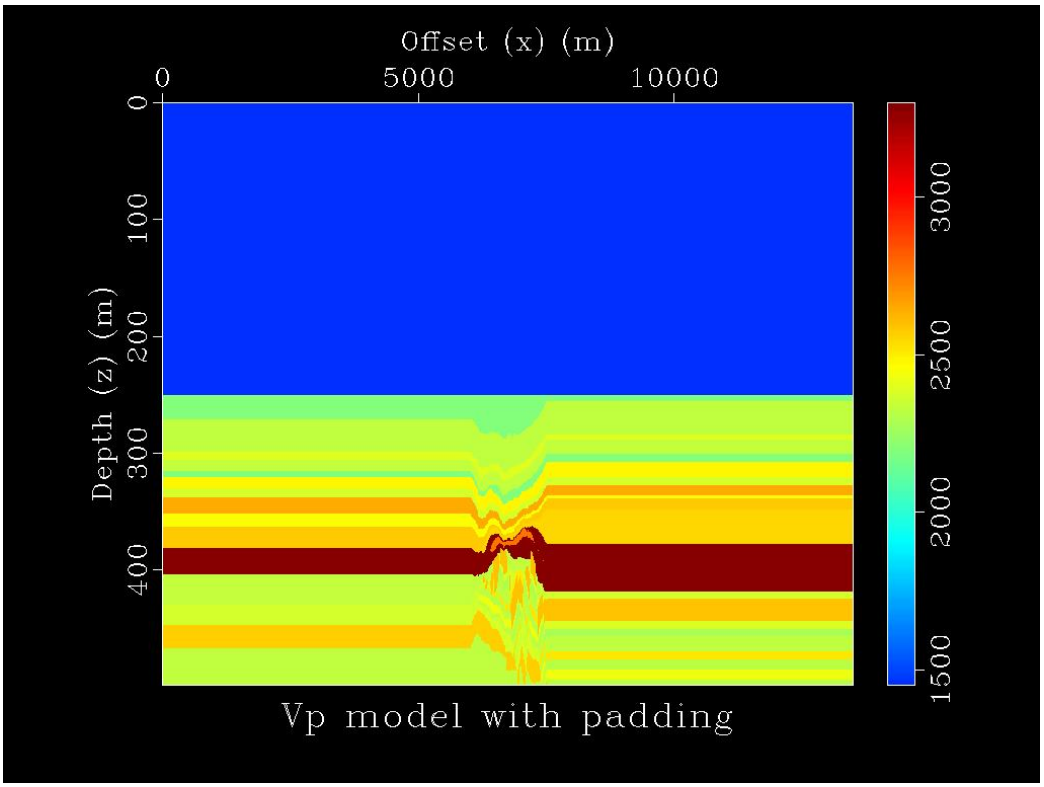

Figure C.2: The P velocity model after 6km of padding has been added at the ends of the model

At it's current version the program requires that the name of the property to be imported is Facies and only one property can be imported at a time however this is easily avoided by just renaming ones properties "Facies" after exporting from Petrel as it is the values for the property one is interested in.

C.1.2 Source Generation

Generating a source is essential in seismic modelling and the method used in this study is to convolve a spike with a ricker wavelet. Creating a spike in

Madagascar is easily done with the program called sfspike and the program sfricker1 preforms the convolution. Figure C.3 shows a spike convolved with a ricker wavelet in Madagascar, in this example the sampling interval (Δ t) was 0.001 seconds was used and a peak frequency 20 Hz was used in the ricker wavelet.

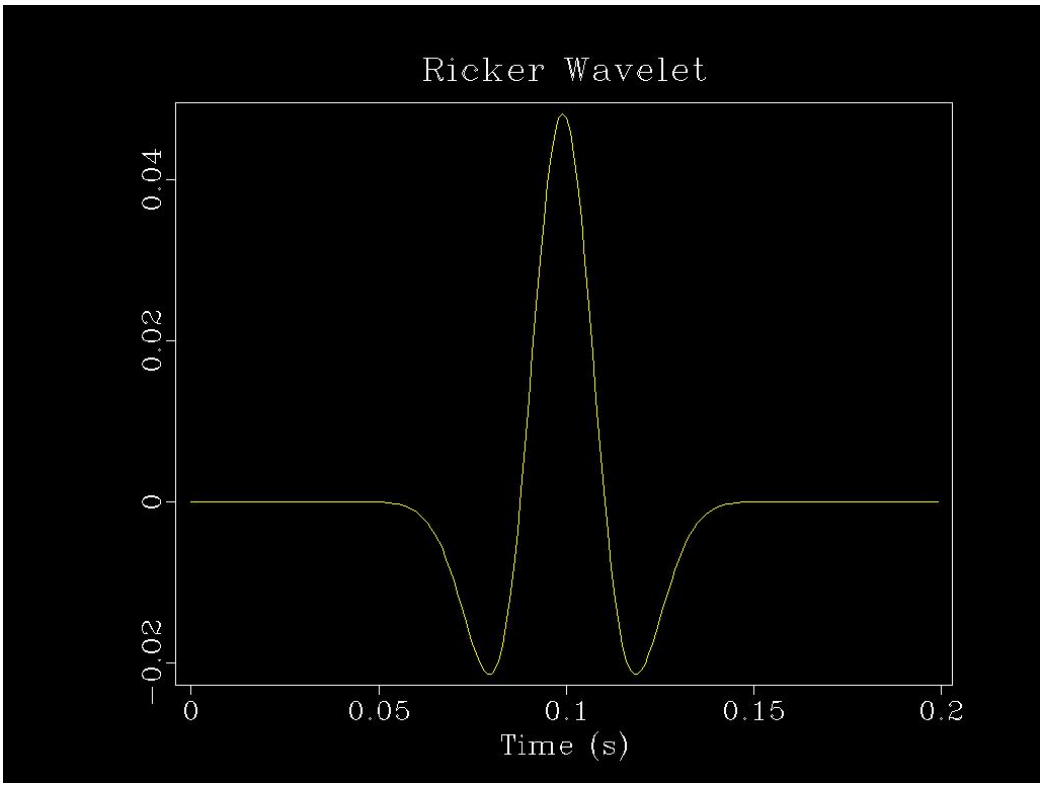

Figure C.3: Spike convolved with ricker wavelet in Madagascar

C.1.3 Forward Seismic Modelling

Several progrmas in the Madgascar pacakge are capable of performing forward seismic modelling and in this thesis the progrmas sffd2dewe and sffwi2dewemodeling are used. The first program is used for single shot modeling while the latter one is used for parallell modeling on cluster nodes and

both progrmas are authored by Espen Birger Raknes and Børge Arntzen of NTNU. In Figure C.4a the program sffd2dewe has been used to perform time-domain 2D finite difference modeling over the model in Figure C.1 and two snaps of the wavefield propagating is shown.

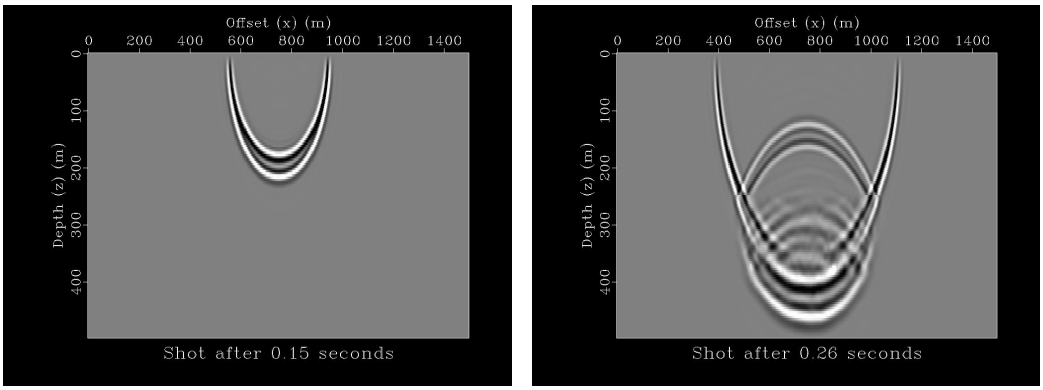

(a) **(b)**

Figure C.4: Two snaps of the propagating wavefield from a shot over the model in Figure C.1 and figure (a) shows a snap after 0.15 seconds and shows the direct wave and the wave reflected from the free surface propagating in the water layer. Figure (b) is taken after 0.26 seconds where the seabottom reflection can be seen propagating upwards, several reflections deeper down in the section can be identified aswell as the main impulse traveling towards the bottom of the section.